Weather-Adaptive Carbon-Aware Optimal Power Flow: Synergizing Dynamic Line Ratings and Meteorological Dispersion via ML-Assisted Optimization

Team 6
IIT Roorkee, Uttarakhand, India

February 2026

Abstract

Standard Carbon-Aware Optimal Power Flow (C-OPF) models currently suffer from a critical "static weather" bias; they treat transmission capacities and generator efficiencies as constant thermal limits and ignore the local meteorological conditions that determine pollutant toxicity. This simplification leads to a grid that is inefficiently constrained during favorable weather, wasting renewable potential, and dangerously permissive during adverse weather, risking acute public health crises.

This paper proposes a **Weather-Adaptive C-OPF (WA-C-OPF)** framework that internalizes real-time meteorological data to co-optimize system cost, global emissions, and local air quality. Our methodology introduces three dynamic mechanisms: **Dynamic Line Ratings (DLR)** to unlock hidden grid capacity using wind cooling; **Temperature-Dependent Generator Efficiency** to penalize thermal plants during heatwaves; and a **Meteorological Dispersion Index (MDI)** to tighten nodal carbon caps during atmospheric stagnation events. To ensure computational tractability, we employ **Machine Learning (ML) Proxies** to map these complex weather-dependent physical interactions into convex constraints compatible with standard solvers.

Implementation and Evaluation: The project will be implemented on the **IEEE 39-bus New England System** by synthesizing historical regional weather data with grid topology. We will first train lightweight regression models to predict safe dynamic line limits and dispersion indices from weather forecasts, decoupling the complex physics from the optimization loop. These ML-predicted parameters will then be integrated into a standard AC-OPF formulation. The proposed model will be evaluated against a static C-OPF baseline using four key metrics: **Renewable Curtailment Reduction**, which measures the energy unlocked by DLR; **Population Exposure (PopEx)**, which quantifies the reduction in health risks during low-dispersion events; **Carbon Abatement Cost**, assessing the economic efficiency of the green transition; and **Constraint Violation Frequency**, determining if the static model would have physically overheated lines that the dynamic model correctly protected.

Keywords: Carbon-Aware OPF, Dynamic Line Rating, Meteorological Dispersion, ML-Assisted Optimization, Nodal Carbon Intensity.

Carbon-Aware Optimal Power Flow

Xin Chen, Andy Sun, Wenbo Shi, Na Li

***Abstract*—To facilitate effective decarbonization of the electric energy sector, this paper introduces a generic Carbon-aware Optimal Power Flow (C-OPF) methodology for power system decision-making that considers the active management of the grid's carbon footprints. Built upon conventional Optimal Power Flow (OPF) models, the proposed C-OPF model further integrates carbon emission flow equations and constraints, as well as carbon-related objectives, to co-optimize electric power flow and carbon emission flow across the power grid. Essentially, the proposed C-OPF can be viewed as a carbon-aware generalization of OPF. Moreover, this paper rigorously establishes the conditions that guarantee the feasibility and solution uniqueness of the carbon emission flow equations, and it proposes a reformulation technique to address the critical issue of undetermined power flow directions in the C-OPF model. Furthermore, two novel carbon footprint models for energy storage systems are developed and incorporated into the C-OPF method. Numerical simulations demonstrate the characteristics and effectiveness of the C-OPF method, in comparison with conventional OPF solutions.**

***Index Terms*—Carbon-aware decision-making, optimal power flow, grid decarbonization, carbon footprint.**

NOMENCLATURE

A. Sets and Parameters

$\mathcal{N}_i$	Set of neighbor nodes of node i.
$\mathcal{N}_i^+(\mathcal{N}_i^-)$	Set of neighbor nodes that send power to (receive power from) node i.
$\mathcal{G}_i$	Set of generators at node i.
$\mathcal{L}_i$	Set of loads at node i.
$\mathcal{T}$	Set of time steps with the time interval δ_t.
$w_{i,g}^{\mathrm{G}}$	Generation carbon emission factor of generator g at node i.

B. Variables

$R_{ij}^i(R_{ij}^j)$	Carbon flow rate of branch ij from node i to node j measured at node i (node j).
R_{ij}^{loss}	Carbon flow rate associated with the power loss of branch ij.
$R_{i,g}^{\mathrm{G}}$	Carbon flow rate from generator g at node i.
$R_{i,l}^{\mathrm{L}}$	Carbon flow rate injected to load l at node i.
$P_{ij}^i(P_{ij}^j)$	Active power flow of branch ij from node i to node j measured at node i (node j).
P_{ij}^{loss}	Power loss of branch ij.
$P_{i,g}^{\mathrm{G}}(Q_{i,g}^{\mathrm{G}})$	Active (reactive) power output of generator g at node i.
$P_{i,l}^{\mathrm{L}}(Q_{i,l}^{\mathrm{L}})$	Active (reactive) power of load l at node i.
$P_{i,t}^{\mathrm{ch}}(P_{i,t}^{\mathrm{dc}})$	Charging (discharging) power of the ES system at node i at time t.
$e_{i,t}^{\mathrm{es}}$	Energy of the ES system at node i at time t.
$E_{i,t}^{\mathrm{es}}$	Virtually stored carbon emissions of the ES system at node i at time t.
$w_{i,t}^{\mathrm{es}}$	Internal carbon emission intensity of the ES system at node i at time t.
w_i	Nodal carbon intensity of node i.

Notes: 1) Notations with an additional subscript t denote the values at time t. For example, $w_{i,t}$ denotes the nodal carbon intensity of node i at time t. 2) For a matrix $\boldsymbol{A}$, $\boldsymbol{A}[i,j]$ denotes the element in i-th row and j-th column.

I. INTRODUCTION

DEEP and rapid decarbonization of electric power systems has emerged as an urgent priority [1] to combat climate change. In 2022, the U.S. electric power sector emitted 1,539 million tons of carbon dioxide (CO_2), which accounts for over 30% of the total U.S. energy-related carbon emissions [2]. To enable transparent and effective grid decarbonization, precisely measuring and quantifying the amount of carbon emissions (i.e., carbon footprints) associated with electricity production and consumption, known as *carbon accounting* [3], is crucial. It lays the quantitative foundation necessary for informing decarbonization decisions, carbon-electricity markets, regulation and policy development. Although almost all carbon emissions in power systems physically originate from electric generators due to the combustion of fossil fuels, it is the electricity consumption that creates the need for power generation and results in emissions. Hence, in addition to accurately measuring the emissions produced by electric generators, it is essential to determine the carbon footprints of end-users by appropriately attribute the generation-side emissions to end-users based on their electricity use, which is referred to as *demand-side carbon accounting* [4]. Accordingly, the Greenhouse Gas (GHG) Protocol[1] [3], [5] establishes two categories of emissions, i.e., Scope 1 and Scope 2, to distinguish the direct generation-side emissions and the indirect (or attributed) emissions associated with electricity consumption and power network losses.

As introduced in [4], carbon accounting frameworks can be categorized into two primary types: *attributional* and *consequential*. *Attributional* carbon accounting aims to allocate direct generation-side emissions to end-users for assigning emissions responsibility, namely the Scope 2 emissions described above. In contrast, *consequential* carbon accounting seeks to evaluate the change or impact on grid emissions resulting from

X. Chen is with the Department of Electrical and Computer Engineering, Texas A&M University, USA; correspondence email: xin_chen@tamu.edu. A. Sun is with the Sloan School of Management and the MIT Energy Initiative, Massachusetts Institute of Technology, USA. W. Shi is with Singularity Energy Inc., USA. N. Li is with the School of Engineering and Applied Sciences, Harvard University, USA.

This work was supported by the NSF ASCENT Award No. 2328241, the Texas A&M Blockchain & Energy Research Consortium, the Texas A&M Smart Grid Center, and the MIT Future Energy Systems Center.

[1]The GHG Protocol [3], [5] developed by the World Resources Institute (WRI) provides internationally recognized GHG accounting and reporting standards and guidelines, which are widely used in the industry.

specific decisions or projects, compared to a counterfactual baseline emission scenario, which employs methods such as *marginal emissions* [6] and avoided emissions. These two carbon accounting frameworks are distinct and serve different purposes [4]. In terms of attributional carbon accounting, there are two main currently-used methods [3]: 1) the location-based method, which adopts grid *average* emission factors (AEFs) across long time horizons and large areas [3], [7] to account for electricity users' carbon footprints, and 2) the market-based method, which derives carbon emission factors purely based on clean power market instruments [8], such as Renewable Energy Certificates (RECs) [9] and Power Purchase Agreement (PPA) [10]. See [4] for a comprehensive overview of carbon accounting methods for power grids.

This paper focuses on the location-based method for attributional demand-side carbon accounting, while the existing AEF-based schemes suffer from two critical limitations: 1) lack of temporal and spatial granularity, and 2) disregard of actual electricity delivery through physical power networks [4]. Since the generation fuel mix in power systems constantly changes over time, the grid carbon intensities of electricity are dynamic and time-varying with significant daily and seasonal patterns [11]. In addition, the grid carbon intensities vary geographically, as generators of different fuel types are distributed across various locations. Moreover, power grids feature specific network topologies and circuits through which power flows, physically connecting end-users with generators and impacting carbon emissions. Therefore, carbon accounting schemes require sufficient granularity and alignment with physical power grids to 1) reflect the temporal variations and spatial diversity in grid emissions, 2) provide precise and accurate carbon accounting results for end-users, and 3) effectively inform and incentivize grid decarbonization decisions. See [4], [7], [12] for more discussions and justifications.

To tackle these issues, the concept of *carbon (emission) flow* is introduced in [13], where carbon emissions are treated as *virtual* network flows embodied in energy flows, transmitted from producers to consumers. References [14], [15] establish the mathematical models of carbon flow in electric power networks. The carbon flow method defines nodal and branch carbon intensities for the grid, providing a temporally and spatially granular depiction of the grid's carbon footprints. In this way, the carbon flow method represents a prominent tool for demand-side carbon accounting, which aligns carbon footprint calculations with the physical grids and power flows. See [14] and Section II for more details. Recent work [16] presents a tree search algorithm to trace the contribution of each generator to individual lines and loads, thereby estimating nodal carbon emissions. This approach builds on the concept of electricity flow tracing [17] and yields nodal carbon emission estimates comparable to those produced by the carbon flow method, with the potential distinction being in how power losses are handled.

Unlike the studies above that focus on accounting for and estimating the grid carbon footprints, this paper aims to advance foundational methodologies for grid decarbonization decision-making and enable optimal carbon-electricity joint management in power grids. In this regard, the *Optimal Power Flow (OPF)* method [18], [19] stands as a foundational mathematical tool for optimizing power system decisions. It has been studied extensively in the literature and widely applied in grid planning, operations, control, and electricity markets [20]–[22]. Existing OPF schemes typically seek optimal power grid decisions to minimize a specific economic cost objective, while satisfying the power flow equations, network constraints, and operational limits of devices. However, the essential goals of grid decarbonization and carbon footprint management are *inadequately* considered. Since power system decisions, e.g., the siting and sizing of renewable generators or power dispatch of various generation sources, directly impact the grid's carbon footprints, it becomes necessary to explicitly integrate carbon footprint management into grid decision-making for achieving desired decarbonization performances and outcomes.

A. Related Work and Key Issues

There have been a number of recent studies [23]–[32] that consider carbon emission flow in power system planning and operation. Reference [23] proposes a transmission expansion planning method that defines an index to quantify the equity performance of carbon emission allocation based on the carbon flow model. In [24], a multi-objective power network transition model is built to plan the retirement of aging coal-fired power plants, while one of the objectives is to minimize user-side carbon footprints. Reference [33] studies the low-carbon operation of multiple energy systems and derives the locational energy-carbon integrated price based on the nodal carbon intensities calculated using the carbon flow method. In [25]–[28], carbon-aware expansion planning models are established for multi-energy systems under carbon emission constraints on electric devices and energy hubs. Additionally, the carbon flow model and constraints are taken into account in power scheduling [29], energy management [30], [31], and peer-to-peer carbon-electricity trading [32]. Existing studies outlined above focus on specific power system applications. However, it remains unaddressed in establishing a fundamental decision-making methodology necessary for guiding various grid decarbonization decisions and supporting theoretical studies and performance analysis.

Moreover, there are two critical issues in the integration of carbon emission flow into the grid decision models that necessitate to be addressed:

1) (*Power Flow Directions*): The carbon flow model [14] needs to pre-determine the power flow directions for all branches to identify the power inflows for each node. However, the directions of branch power flows are typically unknown prior to solving optimal decision models. Most existing works that employ the carbon flow model in grid decision-making either overlook the issue of unknown power flow directions or assume they are predetermined by alternating between grid optimization and carbon flow calculation through iterations [32]. Reference [28] introduces binary indicator variables to handle the unknown power flow directions in the carbon flow model. It results in a mixed-integer nonconvex quadratically constrained optimization problem, which cannot be readily

solved using off-the-shelf optimizers due to involving both integer variables and nonconvex constraints. Thus, a tailored heuristic penalty-based iterative algorithm is designed to solve the optimization problem.

2) (*Carbon Footprint Models for Energy Storage*): By switching between charging and discharging, energy storage (ES) systems can shift load demand and transfer renewable energy across time, offering substantial potential to reduce power system emissions. Hence, developing carbon footprint models for ES systems is crucial, since it lays the quantitative foundation for making optimal ES planning and operation decisions, such as determining installation location and capacity, and managing charging and discharging. In addition, granular and accurate carbon accounting for ES systems enhances information transparency, supporting the development of low-carbon regulatory policies and market mechanisms for ES. It also incentivizes ES stakeholders to adopt low-carbon practices to reduce their own carbon footprint and overall grid emissions. Carbon accounting for ES systems has attracted considerable recent attention from the industry [34], [35]. References [28], [29], [36] propose different carbon footprint models for ES systems, while they neglect the carbon emission leakage associated with ES energy loss (see Remark 4), and the carbon accounting mechanisms for ES system owners remain unclear.

B. Our Contributions

In this paper, we introduce a generic *Carbon-aware Optimal Power Flow (C-OPF)* methodology as the fundamental theory for carbon-aware power system decision-making that incorporates the active management of the grid's carbon footprints. Built upon conventional OPF models, the C-OPF model (see model (7)) further integrates the carbon flow equations and constraints, as well as carbon-related objectives, to co-optimize power flow and carbon flow in the power grid. Essentially, C-OPF is a carbon-aware generalization of OPF, and it produces optimal decisions that satisfy carbon emission constraints and balance the power-related and carbon-related costs. The main contributions of this paper are threefold:

1) To our knowledge, this is the first work that introduces the generic C-OPF methodology and builds its mathematical model for lossy power networks with formulation examples. In particular, this paper rigorously establishes the conditions that guarantee the feasibility and solution uniqueness of the carbon flow equations (see Theorem 1), and presents the key properties of the C-OPF model.
2) We propose a reformulation approach to address the issue of unknown power flow directions in the C-OPF model by introducing dual power flow variables and complementarity constraints. This reformulation is exact and eliminates the necessity of knowing power flow directions in advance.
3) We develop two novel carbon footprint models for ES systems: one precisely models the dynamics of carbon emissions virtually stored in an ES unit and the carbon leakage associated with ES energy loss, while the other treats ES as a load during charging and a carbon-free generator during discharging. The corresponding carbon accounting schemes for ES owners are also introduced.

Furthermore, we develop a carbon-aware economic dispatch model as an example based on the proposed C-OPF method, and demonstrate the effectiveness of C-OPF through numerical experiments in comparison with OPF-based solutions.

Remark 1. *(Key Merits of C-OPF).* In contrast to conventional OPF-based schemes that merely incorporate carbon emission costs into the objective, our proposed C-OPF method possesses three distinct merits: 1) C-OPF explicitly models carbon flow alongside power flow, enabling a *granular* representation and management of the grid's carbon footprints rather than focusing solely on the system-wide total emissions. 2) C-OPF is flexible to model various global and local decarbonization targets or regulatory requirements for different entities and stakeholders. It can ensure that power system decisions comply with these requirements by imposing corresponding carbon flow constraints. 3) C-OPF integrates demand-side carbon accounting mechanisms that attribute emissions from power generation to consumption, which allows the optimization of carbon footprints for end-users, e.g., via carbon-aware power dispatch and demand response. It establishes the theoretical foundation to engage numerous end-users with substantial power flexibility and resources in grid decarbonization decision-making.

The remainder of this paper is organized as follows: Section II introduces the concept and model of carbon flow as well as the use for carbon accounting. Section III presents the C-OPF method with the reformulation approach. Section IV introduces the carbon footprint models for energy storage systems. Numerical experiments are conducted in Section V, and conclusions are drawn in Section VI.

II. Carbon Emission Flow and Carbon Accounting

In this section, we first introduce the concept and model of carbon flow for lossy power networks, and then establish the conditions that ensure the feasibility and solution uniqueness of the carbon flow equations. Next, we present the application of the carbon flow method for demand-side carbon accounting.

A. Concept of Carbon Emission Flow

As mentioned above, the location-based method calculates the average emission factor (i.e., the ratio of total carbon emissions to the total generation energy) of an area grid over a defined period for demand-side carbon accounting. As illustrated in Figure 1, this AEF method treats the power system as a large "pool", assuming that all generations and end-users are connected to one homogeneous and shared infrastructure, without consideration of the power network and power flow. In contrast, the carbon flow method views the carbon emissions from generators as *virtual* attachments to the power flow. These emissions are considered to be transmitted from generators through power networks and accumulate on the user side, forming carbon flows. The concept of carbon flow is analogous to a "*water supply*" system, where virtual

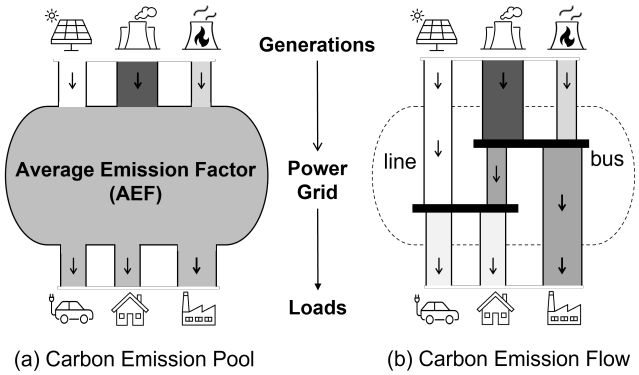

Fig. 1. Comparison between carbon emission pool and carbon emission flow. (In sub-figure (a), all end-users in a large area adopt the same grid average emission factor (AEF) to calculate their attributed carbon footprints. In sub-figure (b), each pipeline represents a power line, with the width indicating the magnitude of power flow. Darker colors indicate higher carbon emission intensities. Power in-flows with different carbon emission intensities are mixed at each bus and distributed downstream.)

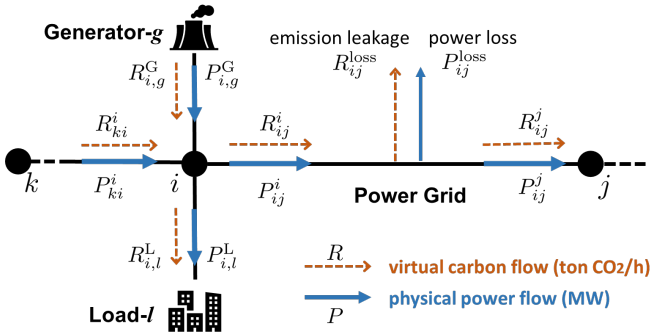

Fig. 2. Illustration of virtual carbon flow and physical power flow.

carbon emissions accompanying power flows can be viewed as invisible particles contained in water flows that are delivered from water sources to users. The carbon emission intensity of electricity is analogous to the particle concentration of water, and a renewable generator is analogous to a pure water source. In this way, the carbon flow method aligns with the physical power grids and underlying power flows, enabling a temporally and spatially granular depiction of the grid's carbon footprints.

In practice, the grid operators and utilities are expected to implement the carbon flow scheme, as these entities oversee power grid operations and possess detailed power flow profiles. Moreover, the carbon flow information (e.g., real-time nodal carbon intensities) represents useful grid emission signals, which can be sent to end-users (e.g., by displaying on smart meters) to inform user-side decarbonization decisions [37].

B. Carbon Emission Flow Model for Lossy Power Networks

Consider a power network described by a connected graph $G(\mathcal{N},\mathcal{E})$, where $\mathcal{N}:=\{1,\cdots,N\}$ denotes the set of nodes and $\mathcal{E}\subset\mathcal{N}\times\mathcal{N}$ denotes the set of branches. As illustrated in Figure 2, the notations with P denote the active power flow values (in the unit of MW), while the notations with R represent the associated carbon flow rates (in the unit of tonCO_2/h). The *carbon (emission) intensity* is defined as the ratio $w=\frac{R}{P}$ (in the unit of tonCO_2/MWh) that describes the amount of carbon flow associated with one unit of power flow.

The active power flows adhere to the power balance equation (1) at each node i:

$$\sum_{k\in\mathcal{N}_i^+} P_{ki}^i + \sum_{g\in\mathcal{G}_i} P_{i,g}^{\mathrm{G}} = \sum_{j\in\mathcal{N}_i^-} P_{ij}^i + \sum_{l\in\mathcal{L}_i} P_{i,l}^{\mathrm{L}}, \quad \forall i\in\mathcal{N}, \quad (1)$$

and $P_{ij}^i = P_{ij}^{\mathrm{loss}} + P_{ij}^j$ for each branch $ij\in\mathcal{E}$. Then, the carbon flow model is built upon the active power flows and the following two fundamental principles [14]:

1) *Conservation Law of Nodal Carbon Mass*: Similar to the power flow balance (1), the total carbon inflows equal the total carbon outflows at each node $i\in\mathcal{N}$, i.e.,

$$\sum_{k\in\mathcal{N}_i^+} R_{ki}^i + \sum_{g\in\mathcal{G}_i} R_{i,g}^{\mathrm{G}} = \sum_{j\in\mathcal{N}_i^-} R_{ij}^i + \sum_{l\in\mathcal{L}_i} R_{i,l}^{\mathrm{L}}. \quad (2)$$

and $R_{ij}^i = R_{ij}^{\mathrm{loss}} + R_{ij}^j$ for each branch $ij\in\mathcal{E}$. In (2), $R_{i,g}^{\mathrm{G}} = w_{i,g}^{\mathrm{G}} P_{i,g}^{\mathrm{G}}$ is the generation carbon emission rate of generator-g at node i.

2) *Proportional Sharing Principle*: At each node $i\in\mathcal{N}$, the allocation of total carbon inflows among all outflows is proportional to their active power flow values, i.e.,

$$R_{ij}^i = \frac{R_i^{\mathrm{in}}}{P_i^{\mathrm{in}}}\cdot P_{ij}^i, \quad R_{i,l}^{\mathrm{L}} = \frac{R_i^{\mathrm{in}}}{P_i^{\mathrm{in}}}\cdot P_{i,l}^{\mathrm{L}}, \quad (3)$$

where $P_i^{\mathrm{in}} := \sum_{k\in\mathcal{N}_i^+} P_{ki}^i + \sum_{g\in\mathcal{G}_i} P_{i,g}^{\mathrm{G}}$ and $R_i^{\mathrm{in}} := \sum_{k\in\mathcal{N}_i^+} R_{ki}^i + \sum_{g\in\mathcal{G}_i} R_{i,g}^{\mathrm{G}}$ denote the total power inflow and total carbon inflow at node $i\in\mathcal{N}$.

The *nodal carbon intensity* of each node i is calculated as (4):

$$w_i = \frac{R_i^{\mathrm{in}}}{P_i^{\mathrm{in}}} = \frac{\sum_{g\in\mathcal{G}_i} w_{i,g}^{\mathrm{G}} P_{i,g}^{\mathrm{G}} + \sum_{k\in\mathcal{N}_i^+} w_k P_{ki}^i}{\sum_{g\in\mathcal{G}_i} P_{i,g}^{\mathrm{G}} + \sum_{k\in\mathcal{N}_i^+} P_{ki}^i}, \ \forall i\in\mathcal{N}, \quad (4)$$

which is the ratio of total carbon inflow to the total power inflow. Equation (4) indicates that the power flow and power loss of each branch $ij\in\mathcal{E}$ share the same carbon emission intensity that equals to the nodal carbon intensity of the sending node, i.e., $\frac{R_{ij}^i}{P_{ij}^i} = \frac{R_{ij}^j}{P_{ij}^j} = \frac{R_{ij}^{\mathrm{loss}}}{P_{ij}^{\mathrm{loss}}} = w_i$.

Equation (4) is referred to as the *carbon flow model* or *carbon flow equation*, and it can be equivalently reformulated in the matrix form (5). The detailed derivation of (5a) is provided in Appendix A.

$$(\boldsymbol{P}_{\mathrm{N}} - \boldsymbol{P}_{\mathrm{B}})\boldsymbol{w}_{\mathrm{N}} = \boldsymbol{r}_{\mathrm{G}} \quad (5a)$$

$$\Longrightarrow \ \boldsymbol{w}_{\mathrm{N}} = (\boldsymbol{P}_{\mathrm{N}} - \boldsymbol{P}_{\mathrm{B}})^{-1}\boldsymbol{r}_{\mathrm{G}}, \quad (5b)$$

Here, $\boldsymbol{w}_{\mathrm{N}} := (w_i)_{i\in\mathcal{N}}\in\mathbb{R}^N$ and $\boldsymbol{r}_{\mathrm{G}} := (\sum_{g\in\mathcal{G}_i} w_{i,g}^{\mathrm{G}} P_{i,g}^{\mathrm{G}})_{i\in\mathcal{N}}\in\mathbb{R}^N$ denote the column vectors that collect the nodal carbon intensities and nodal generation carbon flows, respectively. $\boldsymbol{P}_{\mathrm{N}} := \mathrm{diag}(P_i^{\mathrm{in}})\in\mathbb{R}^{N\times N}$ is the diagonal matrix whose i-th diagonal entry is the nodal active power inflow P_i^{in} to node i. $\boldsymbol{P}_{\mathrm{B}}\in\mathbb{R}^{N\times N}$ is the branch power inflow matrix that is built by letting $\boldsymbol{P}_{\mathrm{B}}[i,k] = P_{ki}^i$ and $\boldsymbol{P}_{\mathrm{B}}[k,i] = 0$ if node k sends power flow P_{ki}^i to node i. Note that P_{ki}^i and P_{ki}^k are different due to the line power loss. Given power flow profiles, the linear equations (5a) can be solved to obtain $\boldsymbol{w}_{\mathrm{N}}$, e.g., through matrix factorization and backward and forward substitution, rather than directly computing the matrix inverse in (5b).

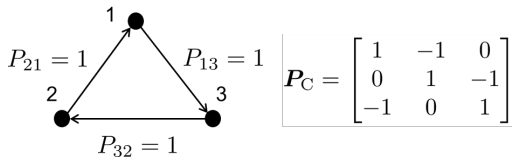

Fig. 3. A simple 3-node network case example.

C. Feasibility and Solution Uniqueness of Carbon Flow Model

A critical fundamental question is whether the carbon flow equations (4) or (5) for a power network are feasible and admit a unique solution. Based on the matrix form (5), it translates to the invertibility of the carbon flow matrix $\boldsymbol{P}_{\mathrm{C}} := \boldsymbol{P}_{\mathrm{N}} - \boldsymbol{P}_{\mathrm{B}}$, which implies the feasibility and solution uniqueness. Hence, this subsection studies the properties of the matrix $\boldsymbol{P}_{\mathrm{C}}$.

By definition, the matrix $\boldsymbol{P}_{\mathrm{C}}$ is diagonally dominant [38], and we define the set $\mathcal{J}$:

$$\mathcal{J} := \Big\{ i \in \mathcal{N} \Big| \, |\boldsymbol{P}_{\mathrm{C}}[i,i]| > \sum_{j=1;j\neq i}^{N} |\boldsymbol{P}_{\mathrm{C}}[i,j]| \Big\}. \tag{6}$$

In practice, $\mathcal{J} \neq \emptyset$, i.e., there exist some rows $i \in \mathcal{J}$ of $\boldsymbol{P}_{\mathrm{C}}$ that are strictly diagonally dominant; such rows correspond to the nodes with generation power injections $P^{\mathrm{G}}_{i,g}$. Then, we establish the *invertibility* property of $\boldsymbol{P}_{\mathrm{C}}$ in Theorem 1.

Theorem 1. *Suppose that for each $i \notin \mathcal{J}$ of the matrix $\boldsymbol{P}_{\mathrm{C}}$, there is a sequence of nonzero elements of $\boldsymbol{P}_{\mathrm{C}}$ of the form $\boldsymbol{P}_{\mathrm{C}}[i,i_1], \boldsymbol{P}_{\mathrm{C}}[i_1,i_2], \cdots, \boldsymbol{P}_{\mathrm{C}}[i_r,j]$ with $j \in \mathcal{J}$. Then, $\boldsymbol{P}_{\mathrm{C}}$ is invertible, and $\boldsymbol{P}_{\mathrm{C}}$ is an M-matrix.*

Proof. According to [39, Theorem], the matrix $\boldsymbol{P}_{\mathrm{C}}$ is nonsingular and thus invertible. Since $\boldsymbol{P}_{\mathrm{C}}$ is diagonally dominant and all its off-diagonal elements $\{\boldsymbol{P}_{\mathrm{C}}[i,j]\}_{i\neq j}$ are non-positive, $\boldsymbol{P}_{\mathrm{C}}$ is an *M-matrix* [40] according to [39, Corollary 4]. □

Theorem 1 indicates that under the condition in Theorem 1, the matrix $\boldsymbol{P}_{\mathrm{C}}$ is invertible, and thus the carbon flow equations are feasible and have a unique solution regarding the nodal carbon intensities and other carbon flow values.

Remark 2. The condition in Theorem 1 can be interpreted as that for any node i with no generation power injection, one can find a power flow path $i \leftarrow i_1 \leftarrow i_2 \leftarrow \cdots \leftarrow i_r \leftarrow j$ in the power network that traces upstream to a node j that has generation power injection. This condition generally holds for practical connected power networks. This condition also implies that every node has non-zero power flux, i.e., $\boldsymbol{P}_{\mathrm{C}}[i,i] > 0$ for all $i \in [N]$. However, non-zero nodal power flux can *not* guarantee that $\boldsymbol{P}_{\mathrm{C}}$ is invertible. For example, consider a simple 3-node circular network case shown in Figure 3. In this case, every node has 1 unit of power flowing through it, but the matrix $\boldsymbol{P}_{\mathrm{C}}$ is singular. And this case violates the condition in Theorem 1. In addition, $\boldsymbol{P}_{\mathrm{C}}$ possesses all the properties of being an *M-matrix*. For example, all the elements of $\boldsymbol{P}_{\mathrm{C}}^{-1}$ are non-negative and every eigenvalue of $\boldsymbol{P}_{\mathrm{C}}$ has a positive real part [40, Theorem 1.1].

D. Use of Carbon Emission Flow for Carbon Accounting

Given power flow results, one can solve the set of carbon flow equations (4) or (5) to obtain the nodal carbon intensities $\boldsymbol{w}_{\mathrm{N}}$, and then calculate all carbon flow values. According to the GHG Protocol [3], [5], the carbon accounting rules are:

- Generator-g at node i shall account for the (Scope 1) direct carbon emission rate $R^{\mathrm{G}}_{i,g} = w^{\mathrm{G}}_{i,g} P^{\mathrm{G}}_{i,g}$;
- Load-l at node i shall account for the (Scope 2) attributed carbon emission rate $R^{\mathrm{L}}_{i,l} = w_i P^{\mathrm{L}}_{i,l}$;
- The power network owner shall account for the (Scope 2) attributed carbon emission rate associated with the network power loss, i.e., $\sum_{ij\in\mathcal{E}} R^{\mathrm{loss}}_{ij} = \sum_{ij\in\mathcal{E}} w_i P^{\mathrm{loss}}_{ij}$.

As the generation fuel mix and power flows change over time, the carbon flow profiles are time-varying, and the carbon footprints over a time period $\mathcal{T}$ (e.g., one day or one year) are the time accumulation of R. For example, the carbon footprint of load-l at node i is calculated as $\hat{E}_{i,l,\mathcal{T}} := \sum_{t\in\mathcal{T}} \delta_t w_{i,t} P^{\mathrm{L}}_{i,l,t}$, where δ_t is the time interval (e.g., 1 hour or 15 minutes).

III. Carbon-Aware Optimal Power Flow Method

In this section, we introduce the generic C-OPF model with examples, and present the reformulation technique to tackle the power flow direction issue of C-OPF.

A. Generic C-OPF Model

To enable the optimal management of carbon footprints in power system decision-making, we propose the generic C-OPF model (7) to co-optimize power flow and carbon flow.

$$\text{Obj.} \quad \min_{\boldsymbol{x}\in\mathcal{X}} \; f_{\mathrm{power}}(\boldsymbol{x},\boldsymbol{y}) + f_{\mathrm{carbon}}(\boldsymbol{x},\boldsymbol{y},\boldsymbol{z}) \tag{7a}$$

$$\text{s.t.} \quad \text{Power Flow Equations } (\boldsymbol{x},\boldsymbol{y}) = \boldsymbol{0}, \tag{7b}$$

$$\text{Power Flow Constraints } (\boldsymbol{y}) \leq \boldsymbol{0}, \tag{7c}$$

$$\text{Carbon Flow Equations } (\boldsymbol{x},\boldsymbol{y},\boldsymbol{z}) = \boldsymbol{0}, \tag{7d}$$

$$\text{Carbon Flow Constraints } (\boldsymbol{x},\boldsymbol{y},\boldsymbol{z}) \leq \boldsymbol{0}. \tag{7e}$$

Here, $\boldsymbol{x}$ denotes the decision variables subject to the feasible set $\mathcal{X}$. The specification of $\boldsymbol{x}$ and $\mathcal{X}$ depends on the practical applications. For instance, $\boldsymbol{x}$ denotes the generation decisions of various generators and $\mathcal{X}$ represents the generation capacity limits and ramping constraints in economic dispatch [41]. $\boldsymbol{x}$ can also be the load adjustment decisions in demand response, or the site and size decisions of new renewable generators in grid planning. $\boldsymbol{y}$ denotes the power flow-related variables, such as network voltage profiles and branch power flows. $\boldsymbol{z}$ represents the carbon flow-related variables, such as nodal carbon intensities $\boldsymbol{w}_{\mathrm{N}}$ and carbon flow values.

1) Objective Function: The objective (7a) aims to minimize the overall cost that consists of two components: the power-related cost denoted as f_{power} and the carbon emission-related cost f_{carbon}. Depending on the specific applications, f_{power} can be the generation cost, network loss, grid expansion investment cost, etc. f_{carbon} is defined to capture the externality of carbon emissions and regulatory penalty on generation-side or demand-side emissions (or the bonus on emission reduction). An example of these cost functions is given by (8):

$$f_{\mathrm{power}} := \sum_{i\in\mathcal{N}} \sum_{g\in\mathcal{G}_i} \Big(c^2_{i,g} (P^{\mathrm{G}}_{i,g})^2 + c^1_{i,g} P^{\mathrm{G}}_{i,g} + c^0_{i,g} \Big), \tag{8a}$$

$$f_{\text{carbon}} := c^{\text{emi}} \cdot \sum_{i\in\mathcal{N}} \sum_{g\in\mathcal{G}_i} w^{\text{G}}_{i,g} P^{\text{G}}_{i,g}, \tag{8b}$$

where (8a) denotes the total generation cost in a quadratic form with the parameters $c^2_{i,g}, c^1_{i,g}, c^0_{i,g}$, and (8b) is the penalty on generation-side emissions with the cost coefficient c^{emi}.

2) Power Flow Equations and Constraints: The power flow equations (7b) and power flow constraints (7c) remain the same as them in classic OPF models [18], [19], [42]. The full AC power flow equations are formulated as (9):

$$\begin{aligned} P^i_{ij} = (V_i^2 - V_i V_j \cos(\theta_i - \theta_j)) g_{ij} \\ - V_i V_j \sin(\theta_i - \theta_j) b_{ij}, \quad \forall ij \in \mathcal{E}, \end{aligned} \tag{9a}$$

$$\begin{aligned} Q^i_{ij} = (V_i V_j \cos(\theta_i - \theta_j) - V_i^2) b_{ij} \\ - V_i V_j \sin(\theta_i - \theta_j) g_{ij}, \quad \forall ij \in \mathcal{E}, \end{aligned} \tag{9b}$$

$$\sum_{j\in\mathcal{N}_i} P^i_{ij} = \sum_{g\in\mathcal{G}_i} P^{\text{G}}_{i,g} - \sum_{l\in\mathcal{L}_i} P^{\text{L}}_{i,l}, \quad \forall i \in \mathcal{N}, \tag{9c}$$

$$\sum_{j\in\mathcal{N}_i} Q^i_{ij} = \sum_{g\in\mathcal{G}_i} Q^{\text{G}}_{i,g} - \sum_{l\in\mathcal{L}_i} Q^{\text{L}}_{i,l}, \quad \forall i \in \mathcal{N}, \tag{9d}$$

where V_i and θ_i are the voltage magnitude and phase angle at node i. Q^i_{ij} denotes the reactive power flow of branch ij from node i to node j measured at node i. g_{ij} and b_{ij} are the conductance and susceptance of branch ij.

The power flow constraints (7c) generally involve the line thermal capacity constraints (10a) and voltage limits (10b).

$$(P^i_{ij})^2 + (Q^i_{ij})^2 \le \bar{S}^2_{ij}, \quad \forall ij \in \mathcal{E}, \tag{10a}$$

$$\underline{V}_i \le V_i \le \bar{V}_i, \quad \forall i \in \mathcal{N}, \tag{10b}$$

where $\bar{S}_{ij}$ is the apparent power capacity of line ij. $\bar{V}_i, \underline{V}_i$ are the upper and lower limits of voltage magnitude at node i.

Since the power flow equations and constraints remain unchanged, the linearization and convexification methods developed for them are still applicable. For instance, the classic DC power flow model (11) [42], which neglects power loss, can be used in the C-OPF model to replace the complete power flow equations (9) for simplicity. In (11a), the superscript "i" is omitted since $P^i_{ij} = P^j_{ij}$ in the DC power flow model due to neglecting power loss.

$$P_{ij} = -b_{ij} \cdot (\theta_i - \theta_j), \quad \forall ij \in \mathcal{E}, \tag{11a}$$

$$\text{Equation (9c)}. \tag{11b}$$

3) Carbon Flow Equations and Constraints: The carbon flow equations (7d) are given by (12):

$$\begin{aligned} w_i \Big(\sum_{g\in\mathcal{G}_i} P^{\text{G}}_{i,g} + \sum_{j\in\mathcal{N}^+_i} P^i_{ji} \Big) \\ = \sum_{g\in\mathcal{G}_i} w^{\text{G}}_{i,g} P^{\text{G}}_{i,g} + \sum_{j\in\mathcal{N}^+_i} w_j P^i_{ji}, \quad \forall i \in \mathcal{N}, \end{aligned} \tag{12}$$

which is simply an equivalent reformulation of (4).

The carbon flow constraints (7e) can take various forms depending on the practical settings for carbon footprint management. For example, an upper limit $\bar{\boldsymbol{w}}_{\text{N}} := (\bar{w}_i)_{i\in\mathcal{N}}$ can be imposed on nodal carbon intensities, i.e. (13), to ensure that users at these nodes are supplied with low-carbon electricity. By adjusting this upper limit $\bar{\boldsymbol{w}}_{\text{N}}$, one can control the level of "cleanness" of the supplied electricity at a certain location. In particular, letting $\bar{w}_i = 0$ enforces that the electricity supply at node i is completely carbon-free. The definition of "node" is flexible in terms of geographical scales, which can represent a district grid, a distribution feeder, or a balancing area.

$$w_i \le \bar{w}_i, \quad \forall i \in \mathcal{N}. \tag{13}$$

An alternative carbon flow constraint (7e) can impose a cap $\bar{E}^{\text{L}}_{i,l}$ on the total individual user-side emissions as (14):

$$\delta_t \sum_{t\in\mathcal{T}} (w_{i,t} \cdot P^{\text{L}}_{i,l,t}) \le \bar{E}^{\text{L}}_{i,l}, \quad \forall l \in \mathcal{L}_i, i \in \mathcal{N}. \tag{14}$$

Besides, instead of an emission cap on individual users, a cap $\bar{E}^{\text{L}}_i$ on the total nodal level emissions can be imposed as (15):

$$\delta_t \sum_{t\in\mathcal{T}} \Big(w_{i,t} \cdot \sum_{l\in\mathcal{L}_i} P^{\text{L}}_{i,l,t} \Big) \le \bar{E}^{\text{L}}_i, \quad \forall i \in \mathcal{N}. \tag{15}$$

The determination of the cap parameters depends on practical requirements. Other carbon flow constraints, including requirement for emission allocation fairness and equity [23], can also be employed.

Due to the proportional sharing principle used in the carbon flow model, a natural limit on nodal carbon intensities is $w_i \in [0, w^{\text{G}}_{\max}]$ for all $i \in \mathcal{N}$, where $w^{\text{G}}_{\max} := \max_{i,g}\{w^{\text{G}}_{i,g}\}$ is the largest generation carbon emission factor. Hence, if $\bar{w}_i$ in (13) is set to be larger than $w^{\text{G}}_{\max}$ for some nodes i, (13) imposes no actual constraint on these nodes. Another critical issue is that inappropriately designed carbon flow constraints may render the C-OPF model (7) infeasible, e.g., when the caps in (13)-(15) are too small to be achievable. To address this issue, the hard constraints (13)-(15) can be converted to soft constraints by adding slack variables with corresponding penalties in the objective. For example, one can replace constraint (15) with (16) and add a penalty term $\sum_{i\in\mathcal{N}}(c^{\text{E}}_i \cdot \alpha_i)$ to the carbon-related cost function f_{carbon} in objective (7a):

$$\delta_t \sum_{t\in\mathcal{T}} \Big(w_{i,t} \sum_{l\in\mathcal{L}_i} P^{\text{L}}_{i,l,t} \Big) \le \bar{E}^{\text{L}}_i + \alpha_i, \ \alpha_i \ge 0, \quad \forall i \in \mathcal{N}, \tag{16}$$

where α_i is the slack variable and c^{E}_i denotes the penalty cost coefficient for excessive demand-side emissions.

Remark 3. We note that the carbon flow constraints are not inherent physical limitations but rather regulatory requirements imposed on the power grid and end-users to manage their carbon footprints. The objective is to incentivize low-carbon electricity supply and consumption behaviors and ensure compliance with grid decarbonization regulations and targets. For instance, to meet the emission cap constraints (14), (15), end-users can optimally schedule their load trajectories $(P^{\text{L}}_{i,l,t})_{t\in\mathcal{T}}$ to increase (decrease) electricity consumption when the grid exhibits low (high) nodal carbon intensity. Alternatively, additional renewable generation units can be deployed in proximity to node i, to effectively reduce the nodal carbon intensity $w_{i,t}$. These lead to the development of optimal carbon-aware demand response and expansion planning schemes based on the C-OPF method, and it can also be used to support many other carbon-aware decision applications in power systems. □

Essentially, the C-OPF model (7) is a carbon-aware generalization of the OPF model, and it reduces to an OPF model

if the carbon-related objective function f_{carbon}, carbon flow equations (7d) and constraints (7e) are removed or inactive. It also implies that existing OPF techniques, such as linearization, convexification, decomposition, stochastic modeling, etc., can still be applied to the power flow components in C-OPF (7). Moreover, the C-OPF model (7) can be directly extended to the multi-period settings and involve time-coupled constraints, such as generator ramping limits and the state-of-charge constraints of ES systems. As an illustrative example, a multi-period C-OPF-based economic dispatch model (27) is established in Section V-A, which includes these time-coupled constraints and employs a full AC power flow model.

In the C-OPF model (7), the carbon flow method is used for demand-side carbon accounting to align the grid's carbon footprint quantification with physical power system operation and actual power flows. Nevertheless, the C-OPF method is flexible and can adapt to other carbon accounting approaches by replacing the carbon flow equation (7d) with other valid carbon accounting mathematical models.

B. Reformulation for Power Flow Directions

As mentioned in the introduction section and indicated by the set $\mathcal{N}_i^+$, the carbon flow equation (12) requires the predetermination of branch power flow directions to identify the power inflows for each node. However, the directions of branch power flows are generally unknown prior to solving the C-OPF problem. To address this issue, we introduce two non-negative power flow variables $\hat{P}^i_{ji} \geq 0$ and $\hat{P}^i_{ij} \geq 0$ for each branch $ij \in \mathcal{E}$ with $P^i_{ij} = \hat{P}^i_{ij} - \hat{P}^i_{ji}$. Specifically, $\hat{P}^i_{ji}$ and $\hat{P}^i_{ij}$ denote the power flow components from node j to node i and from node i to node j, respectively, both of which are measured on the side of node i. Then, we can equivalently reformulate the carbon flow equation (12) as (17), and also need to replace P^i_{ij} with $\hat{P}^i_{ij} - \hat{P}^i_{ji}$ in the power flow equations (9) (or the DC power flow model (11)) and constraints (10a).

$$w_i\Big(\sum_{g\in\mathcal{G}_i} P^{\mathrm{G}}_{i,g} + \sum_{j\in\mathcal{N}_i} \hat{P}^i_{ji}\Big) = \sum_{g\in\mathcal{G}_i} w^{\mathrm{G}}_{i,g} P^{\mathrm{G}}_{i,g} + \sum_{j\in\mathcal{N}_i} w_j \hat{P}^i_{ji}, \qquad \forall i \in \mathcal{N}, \tag{17a}$$

$$\hat{P}^i_{ji} \geq 0, \ \ \hat{P}^i_{ij} \geq 0, \qquad \forall ij \in \mathcal{E}, \tag{17b}$$

$$\hat{P}^i_{ji} \cdot \hat{P}^i_{ij} = 0, \qquad \forall ij \in \mathcal{E}. \tag{17c}$$

In (17a), we replace $\mathcal{N}_i^+$ (the set of neighbor nodes that send power to node i) by $\mathcal{N}_i$ (the set of all neighbor nodes of node i). In addition, the complementarity constraint (17c) is added to ensure that either $\hat{P}^i_{ji}$ or $\hat{P}^i_{ij}$ must be zero for each branch ij. Here, a useful trick to facilitate the nonlinear optimization is to replace the complementarity constraint (17c) by the relaxed constraint (18) [43], and this relaxation is exact due to (17b).

$$\hat{P}^i_{ji} \cdot \hat{P}^i_{ij} \leq 0, \qquad \forall ij \in \mathcal{E}. \tag{18}$$

Alternatively, we can introduce a binary variable γ_{ij} for $ij \in \mathcal{E}$ and linearize the complementarity constraint (17c) with

$$\gamma_{ij} \in \{0,1\}, \ \ \hat{P}^i_{ji} \leq (1-\gamma_{ij})\bar{P}_{ij}, \ \ \hat{P}^i_{ij} \leq \gamma_{ij}\bar{P}_{ij}. \tag{19}$$

Note that both reformulations via (17) or (19) are equivalent to the original carbon flow equation (12), but the branch flow directions do not need to be known in advance.

In [28], binary indicator variables are introduced to handle the unknown power flow directions in the carbon flow model. It results in a mixed-integer nonconvex quadratically constrained optimization problem, and a tailored penalty-based iterative algorithm is designed in [28] to solve the optimization problem through a number of iterations. In contrast, our proposed dual power flow variables reformulation method with the complementarity constraints (18) renders the C-OPF model a standard nonconvex optimization problem without integer variables. Therefore, the C-OPF model can be directly solved using off-the-shelf nonlinear optimizers such as IPOPT [44], without the need for designing ad hoc solution algorithms.

IV. Carbon Footprint Model for Energy Storage

Energy storage (ES) systems play a critical role in decarbonizing power grids, as their operations can be optimized to curtail overall system emissions, e.g., charging when the grid is clean and discharging when the grid is under high emissions. Consider an ES system connected to node $i \in \mathcal{N}$. For time $t \in \mathcal{T} := \{1, 2, \cdots, T\}$ with the time interval δ_t, the dynamical ES power model [45] is formulated as (20):

$$0 \leq P^{\mathrm{ch}}_{i,t} \leq \bar{P}^{\mathrm{ch}}_i, \quad 0 \leq P^{\mathrm{dc}}_{i,t} \leq \bar{P}^{\mathrm{dc}}_i, \tag{20a}$$

$$P^{\mathrm{ch}}_{i,t} \cdot P^{\mathrm{dc}}_{i,t} = 0, \tag{20b}$$

$$e^{\mathrm{es}}_{i,t+1} = \kappa_i e^{\mathrm{es}}_{i,t} + \delta_t\big(\eta^{\mathrm{ch}}_i P^{\mathrm{ch}}_{i,t} - \frac{1}{\eta^{\mathrm{dc}}_i} P^{\mathrm{dc}}_{i,t}\big), \tag{20c}$$

$$\underline{e}_i \leq e^{\mathrm{es}}_{i,t} \leq \bar{e}_i, \quad e^{\mathrm{es}}_{i,T+1} = e^{\mathrm{es}}_{i,1}, \quad \forall i \in \mathcal{N}, t \in \mathcal{T}. \tag{20d}$$

Here, $\bar{P}^{\mathrm{ch}}_i$ and $\bar{P}^{\mathrm{dc}}_i$ are the charging and discharging power capacities. $\eta^{\mathrm{ch}}_i \in (0,1]$ and $\eta^{\mathrm{dc}}_i \in (0,1]$ denote the charging and discharging efficiency coefficients, respectively. $\kappa_i \in (0,1]$ denotes the storage efficiency factor that models the loss of stored energy over time. $\bar{e}_i$ and $\underline{e}_i$ are the upper and lower bounds of the energy level of the ES system. The complementarity constraint (20b) is used to enforce that an ES unit can not charge and discharge at the same time.

In this section, we propose two carbon footprint models for ES systems: the "water tank" model and the "load/carbon-free generator" model. The associated carbon accounting mechanisms for ES owners are presented as well.

A. "Water Tank" Carbon Footprint Model

The "water tank" model of ES is conceptually aligned with the analogy of a "water supply" system used to explain the carbon flow model in Section II-A. Analogous to a water tank that stores both water and invisible particles, an ES system is viewed to store both electric energy $e^{\mathrm{es}}_{i,t}$ (in the unit of MWh) and *virtual* carbon emissions $E^{\mathrm{es}}_{i,t}$ (in the unit of tonCO_2). We then define the internal ES carbon intensity $w^{\mathrm{es}}_{i,t}$ as (21):

$$w^{\mathrm{es}}_{i,t} = \frac{E^{\mathrm{es}}_{i,t}}{e^{\mathrm{es}}_{i,t}}. \tag{21}$$

Note that $e^{\mathrm{es}}_{i,t}$ should not be zero to make $w^{\mathrm{es}}_{i,t}$ well-defined. This can be achieved by setting the lower energy bound $\underline{e}_i$ in

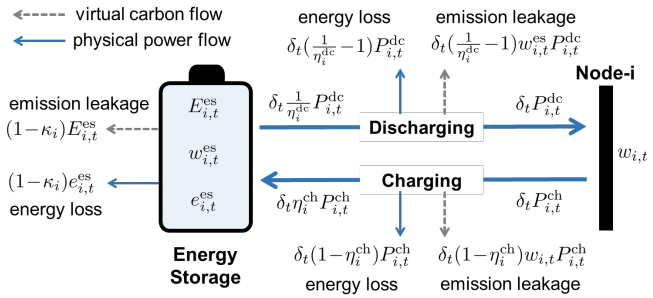

Fig. 4. Power flow and carbon flow under the "water tank" ES model.

(20d) to be a small positive value rather than zero. It can also prevent numerical issues during the optimization process.

Based on the ES power model (20), we develop the dynamical *carbon footprint model of* the ES unit as (22) for $t \in \mathcal{T}$:

$$E^{\mathrm{es}}_{i,t+1} = \kappa_i E^{\mathrm{es}}_{i,t} + \delta_t \big(w_{i,t} \eta^{\mathrm{ch}}_i P^{\mathrm{ch}}_{i,t} - w^{\mathrm{es}}_{i,t} \frac{1}{\eta^{\mathrm{dc}}_i} P^{\mathrm{dc}}_{i,t} \big). \tag{22}$$

Model (22) implies that (virtual) carbon emissions are injected into the ES unit when it charges with electricity in the nodal carbon intensity $w_{i,t}$; and it releases the stored emissions back to the grid when it discharges with electricity in the ES carbon intensity $w^{\mathrm{es}}_{i,t}$. In particular, (22) models the *carbon emission leakage* associated with the energy loss during the storage, charging, and discharging processes of the ES unit. Figure 4 illustrates the carbon flow and power flow of the ES unit.

Alternatively, we can plug in the ES carbon intensity (21) into (22) to eliminate the variable $E^{\mathrm{es}}_{i,t}$ and reformulate the ES carbon footprint model *equivalently* as (23):[2]

$$w^{\mathrm{es}}_{i,t+1} = \lambda_{i,t} \cdot w^{\mathrm{es}}_{i,t} + (1 - \lambda_{i,t}) \cdot w_{i,t}, \tag{23a}$$

$$\lambda_{i,t} := \frac{\kappa_i e^{\mathrm{es}}_{i,t}}{\kappa_i e^{\mathrm{es}}_{i,t} + \delta_t \eta^{\mathrm{ch}}_i P^{\mathrm{ch}}_{i,t}}, \tag{23b}$$

which describes the dynamics of the ES carbon intensity $w^{\mathrm{es}}_{i,t}$. Interestingly, equation (23a) indicates an intuitive feature that the ES carbon intensity $w^{\mathrm{es}}_{i,t+1}$ at the next time $t+1$ is a *convex combination* of the ES carbon intensity $w_{i,t}$ at time t and the nodal carbon intensity $w_{i,t}$ with the weight coefficient $\lambda_{i,t} \in [0,1]$. When charging, the ES unit behaves as if mixing the internally stored electricity with the newly charged electricity; when it discharges, $\lambda_{i,t} = 1$ and the ES carbon intensity remains unchanged, i.e., $w^{\mathrm{es}}_{i,t+1} = w^{\mathrm{es}}_{i,t}$.

Accordingly, the carbon flow equation (17a) in the C-OPF model is modified as (24) to incorporate the ES system.

$$w_{i,t}\big(P^{\mathrm{dc}}_{i,t} + \sum_{g \in \mathcal{G}_i} P^{\mathrm{G}}_{i,g,t} + \sum_{j \in \mathcal{N}_i} \hat{P}^{i}_{ji,t}\big) = w^{\mathrm{es}}_{i,t} P^{\mathrm{dc}}_{i,t} + \sum_{g \in \mathcal{G}_i} w^{\mathrm{G}}_{i,g,t} P^{\mathrm{G}}_{i,g,t} + \sum_{j \in \mathcal{N}_i} w_{j,t} \hat{P}^{i}_{ji,t}, \quad \forall i \in \mathcal{N}, t \in \mathcal{T}. \tag{24}$$

From (24), it is seen that an ES unit affects the nodal carbon intensities and carbon flow only when it discharges.

[2]In (23b), the term $\frac{\delta_t}{\eta^{\mathrm{dc}}_i} P^{\mathrm{dc}}_{i,t}$ is dropped from the definition of $\lambda_{i,t}$, because $P^{\mathrm{dc}}_{i,t} = 0$ when the ES unit charges and $\lambda_{i,t} = 1$ when it discharges, which are not affected by this term.

Remark 4. *(Comparison with Existing ES Emission Models).* Existing carbon emission models for ES systems proposed in [28], [29], [36] also formulate the virtually stored emissions and internal ES carbon intensity. However, these models neglect the carbon emission leakage associated with the energy loss during the storage, charging, and discharging processes. This issue makes these ES carbon emission models not rigorous or even problematic. For example, consider the scenario when an ES unit remains idle, i.e., neither charging nor discharging. Over time, the stored energy e_t gradually depletes to zero due to energy loss, while the virtually stored carbon emissions E_t remain constant as the carbon leakage associated with energy loss is not considered. As a result, the internal ES carbon intensity E_t/e_t would approach an infinitely large value, which is unreasonable. In contrast, our proposed "water tank" ES carbon footprint model (22) or (23) avoids these issues by precisely modeling carbon leakage, ensuring that carbon footprint attribution is consistent with the actual electric energy usage. □

Remark 5. *(Carbon Accounting for ES Owners).* Under the "water tank" carbon footprint model, for the time horizon $\mathcal{T}$, the owner of the ES system shall account for the (Scope 2) attributed carbon emission $\hat{E}^{\mathrm{es}}_{i,\mathcal{T}}$ that is calculated by (25):

$$\hat{E}^{\mathrm{es}}_{i,\mathcal{T}} = \sum_{t=1}^{T} \delta_t (w_{i,t} P^{\mathrm{ch}}_{i,t} - w^{\mathrm{es}}_{i,t} P^{\mathrm{dc}}_{i,t}), \quad \forall i \in \mathcal{N}, \tag{25}$$

which is the net carbon emissions withdrawn from the grid. Intuitively, the attributed emission $\hat{E}^{\mathrm{es}}_{i,\mathcal{T}}$ can be decomposed into two parts: 1) the change of virtually stored carbon emissions, i.e., $E^{\mathrm{es}}_{i,T+1} - E^{\mathrm{es}}_{i,1}$, and 2) the carbon emission leakage associated with ES energy loss, i.e., $E^{\mathrm{es}}_{i,1} + \sum_{t=1}^{T} \delta_t (w_{i,t} P^{\mathrm{ch}}_{i,t} - w^{\mathrm{es}}_{i,t} P^{\mathrm{dc}}_{i,t}) - E^{\mathrm{es}}_{i,T+1}$. To make it more clear, we consider a lossless ES unit with $\kappa_i = \eta^{\mathrm{ch}}_i = \eta^{\mathrm{dc}}_i = 1$. If this ES unit recovers the initially stored emission level in the final time step, namely $E^{\mathrm{es}}_{i,T+1} = E^{\mathrm{es}}_{i,1}$, we have $\hat{E}^{\mathrm{es}}_{i,\mathcal{T}} = E^{\mathrm{es}}_{i,T+1} - E^{\mathrm{es}}_{i,1} = 0$ from (22). In this case, the ES owner accounts for *zero* carbon emissions, regardless of the number of charging and discharging cycles. This outcome aligns with the role of an ES system, which does not directly produce or consume electricity (carbon emissions) itself but rather enables the temporal shifts. □

B. "Load/Carbon-Free Generator" Carbon Footprint Model

The proposed "water tank" model above requires continuous monitoring of the virtually stored carbon emissions within an ES system. To facilitate practical implementation, we propose an alternative model termed "*load/carbon-free generator*" to characterize the carbon footprints of an ES unit. Specifically, this model directly treats an ES unit as a load during charging and as a carbon-free clean generator during discharging. Accordingly, the carbon flow equation (17a) in the C-OPF model is modified as (24) with $w^{\mathrm{es}}_{i,t} \equiv 0$ for all t, since the ES unit is regarded as a carbon-free generator during discharging.

In terms of carbon accounting, under the "load/carbon-free generator" model, the ES owner shall account for the (Scope

2) attributed carbon emissions $\hat{E}^{\text{es}}_{i,\mathcal{T}}$ calculated by (26):

$$\hat{E}^{\text{es}}_{i,\mathcal{T}} = \sum_{t=1}^{T} \delta_t w_{i,t} P^{\text{ch}}_{i,t}, \qquad \forall i \in \mathcal{N}. \tag{26}$$

It implies that the virtual carbon emissions absorbed from the grid during the charging period accumulate locally at the ES unit and are not released back to the grid. Thus, the ES owner incurs higher Scope-2 carbon emissions compared with the carbon accounting scheme (25) under the "water tank" model. Nevertheless, under the "load/carbon-free generator" model, ES owners can make profits by acting as clean energy suppliers in the carbon-electricity market, e.g., selling renewable energy certificates (RECs) [9], since the discharging power is considered carbon-free. As a result, ES owners are incentivized to charge their ES units when the grid is clean with low carbon intensity to reduce their own carbon footprints (26); and they are incentivized to discharge when the grid is in high emission to make more profit, as the price of clean electricity or RECs is expected to be higher at that time. In this way, the "load/carbon-free generator" model is easy to use and naturally incentivizes the carbon-aware operation of ES systems. The simulation comparison between the "water tank" and "load/carbon-free generator" ES carbon footprint models are provided in Section V-E.

We note that alongside the two proposed carbon footprint models for ES systems, there could be other valid models. The use of different carbon models can lead to discrepancies in carbon accounting results, operational decision-making, and market design for ES systems. Hence, it is crucial to assess the impact and select an appropriate model that aligns with practical objectives and specific requirements.

V. Numerical Experiments

In this section, we build a carbon-aware economic dispatch model based on the C-OPF method as an example for numerical tests, comparing it with conventional OPF-based schemes.

A. C-OPF-Based and OPF-Based Economic Dispatch Models

Based on the C-OPF method (7), we develop a carbon-aware economic dispatch (C-ED) model (27) as a specific application example. It involves the multi-period optimal power scheduling of various generators and ES systems, while considering a complete AC power flow model, network operational constraints, and carbon flow equations and constraints. The C-ED model (27) is formulated as a nonconvex optimization problem and we solve it using the solver IPOPT [44].

$$\text{Obj.} \ \min \sum_{i\in\mathcal{N}}\sum_{t\in\mathcal{T}}\Big[\sum_{g\in\mathcal{G}_i}\big(c^2_{i,g}(P^{\text{G}}_{i,g,t})^2 + c^1_{i,g}P^{\text{G}}_{i,g,t} + c^0_{i,g}\big) + c^{\text{es}}_i(P^{\text{dc}}_{i,t} + P^{\text{ch}}_{i,t})\Big], \tag{27a}$$

$$\text{s.t.} \ \underline{P}^{\text{G}}_{i,g,t} \le P^{\text{G}}_{i,g,t} \le \bar{P}^{\text{G}}_{i,g,t}, \qquad \forall i\in\mathcal{N}, g\in\mathcal{G}_i, t\in\mathcal{T} \tag{27b}$$

$$\underline{Q}^{\text{G}}_{i,g,t} \le Q^{\text{G}}_{i,g,t} \le \bar{Q}^{\text{G}}_{i,g,t}, \qquad \forall i\in\mathcal{N}, g\in\mathcal{G}_i, t\in\mathcal{T} \tag{27c}$$

$$\underline{\Delta}^{\text{G}}_{i,g} \le P^{\text{G}}_{i,g,t} - P^{\text{G}}_{i,g,t-1} \le \bar{\Delta}^{\text{G}}_{i,g}, \ \forall i\in\mathcal{N}, g\in\mathcal{G}_i, t\in\mathcal{T} \tag{27d}$$

$$\hat{P}^i_{ij,t} - \hat{P}^i_{ji,t} = \big(V^2_{i,t} - V_{i,t}V_{j,t}\cos(\theta_{i,t}-\theta_{j,t})\big)g_{ij} - V_{i,t}V_{j,t}\sin(\theta_{i,t}-\theta_{j,t})b_{ij}, \qquad \forall ij\in\mathcal{E}, t\in\mathcal{T} \tag{27e}$$

$$\hat{P}^j_{ij,t} - \hat{P}^j_{ji,t} = -\big(V^2_{j,t} - V_{j,t}V_{i,t}\cos(\theta_{j,t}-\theta_{i,t})\big)g_{ij} + V_{j,t}V_{i,t}\sin(\theta_{j,t}-\theta_{i,t})b_{ij}, \qquad \forall ij\in\mathcal{E}, t\in\mathcal{T} \tag{27f}$$

$$Q^i_{ij,t} = \big(V_{i,t}V_{j,t}\cos(\theta_{i,t}-\theta_{j,t}) - V^2_{i,t}\big)b_{ij} - V_{i,t}V_{j,t}\sin(\theta_{i,t}-\theta_{j,t})g_{ij}, \qquad \forall ij\in\mathcal{E}, t\in\mathcal{T} \tag{27g}$$

$$Q^j_{ij,t} = -\big(V_{j,t}V_{i,t}\cos(\theta_{j,t}-\theta_{i,t}) - V^2_{j,t}\big)b_{ij} + V_{j,t}V_{i,t}\sin(\theta_{j,t}-\theta_{i,t})g_{ij}, \qquad \forall ij\in\mathcal{E}, t\in\mathcal{T} \tag{27h}$$

$$\sum_{g\in\mathcal{G}_i} P^{\text{G}}_{i,g,t} - P^{\text{L}}_{i,t} + P^{\text{dc}}_{i,t} - P^{\text{ch}}_{i,t} = \sum_{j\in\mathcal{N}_i}(\hat{P}^i_{ij,t} - \hat{P}^i_{ji,t}), \qquad \forall i\in\mathcal{N}, t\in\mathcal{T} \tag{27i}$$

$$\sum_{g\in\mathcal{G}_i} Q^{\text{G}}_{i,g,t} - Q^{\text{L}}_{i,t} = \sum_{j\in\mathcal{N}_i} Q^i_{ij,t}, \qquad \forall i\in\mathcal{N}, t\in\mathcal{T} \tag{27j}$$

$$(\hat{P}^i_{ij,t} - \hat{P}^i_{ji,t})^2 + (Q^i_{ij,t})^2 \le \bar{S}^2_{ij}, \qquad \forall ij\in\mathcal{E}, t\in\mathcal{T} \tag{27k}$$

$$(\hat{P}^j_{ij,t} - \hat{P}^j_{ji,t})^2 + (Q^j_{ij,t})^2 \le \bar{S}^2_{ij}, \qquad \forall ij\in\mathcal{E}, t\in\mathcal{T} \tag{27l}$$

$$\underline{V}_i \le V_{i,t} \le \bar{V}_i, \ \underline{\theta}_i \le \theta_{i,t} \le \bar{\theta}_i, \qquad \forall i\in\mathcal{N}, t\in\mathcal{T} \tag{27m}$$

$$0 \le \hat{P}^i_{ij,t}, 0 \le \hat{P}^i_{ji,t}, \ \hat{P}^i_{ij,t}\cdot\hat{P}^i_{ji,t} \le 0, \qquad \forall ij\in\mathcal{E}, t\in\mathcal{T} \tag{27n}$$

$$0 \le \hat{P}^j_{ij,t}, 0 \le \hat{P}^j_{ji,t}, \ \hat{P}^j_{ij,t}\cdot\hat{P}^j_{ji,t} \le 0, \qquad \forall ij\in\mathcal{E}, t\in\mathcal{T} \tag{27o}$$

$$w_{i,t} \le \bar{w}_{i,t}, \qquad \forall i\in\mathcal{N}, t\in\mathcal{T} \tag{27p}$$

$$\text{Equations (20), (23), (24).} \tag{27q}$$

The objective (27a) aims to minimize the total generation and ES operational costs, where c^{es}_i denotes the ES degradation cost coefficient. Equations (27b)-(27d) denote the active and reactive power generation capacity limits and the ramping constraints for various generators. Equations (27e) and (27f) represent the full AC power flow equations for the active power flow values at the sending and receiving nodes, respectively. Here, we employ the dual power flow reformulation method introduced in Section III-B to address the issue of unknown power flow directions. As shown in Figure 2, $P^i_{ij,t} = \hat{P}^i_{ij,t} - \hat{P}^i_{ji,t}$ and $P^j_{ij,t} = \hat{P}^j_{ij,t} - \hat{P}^j_{ji,t}$ are the active power flow values of branch ij that are measured at node i and node j, respectively. Thus, the power loss of branch ij is $P^{\text{loss}}_{ij,t} = |P^i_{ij,t} - P^j_{ij,t}|$. Similarly, equations (27g) and (27h) represent the full AC power flow equations for the branch reactive power flows at the sending and receiving nodes, respectively. Equations (27i) and (27j) are the active and reactive power balance constraints at each node. Equations (27k) and (27l) represent the line thermal constraints at the sending and receiving nodes, respectively. Equation (27m) denotes the upper and lower limits on nodal voltage magnitudes and phase angles. Equations (27n) and (27o) represent the nonnegativity and complementarity constraints for the dual power flow values; see Section III-B for more explanations. Equation (27p) is the carbon flow constraint that imposes a cap on the nodal carbon intensities. This constraint enables the active management of nodal carbon intensities, ensuring that clean power is supplied to users with a carbon intensity no greater than $\bar{w}_{i,t}$. Equation (27q) collects the dynamic power model (20) and the "water tank" carbon emission model (23) for ES systems, as well as the carbon flow equations (24).

For comparison, we also build a conventional OPF-based

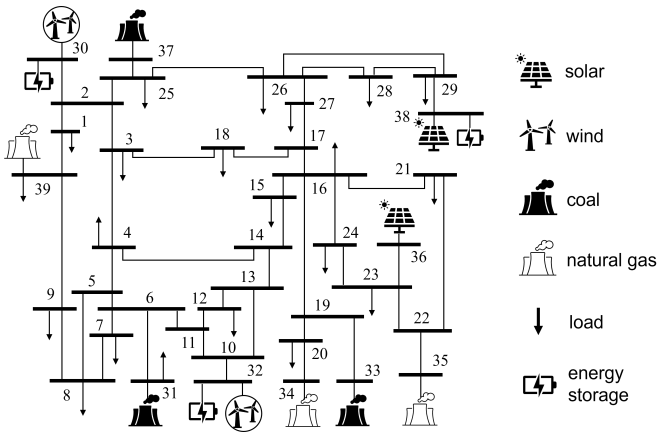

Fig. 5. The modified New England 39-bus test system.

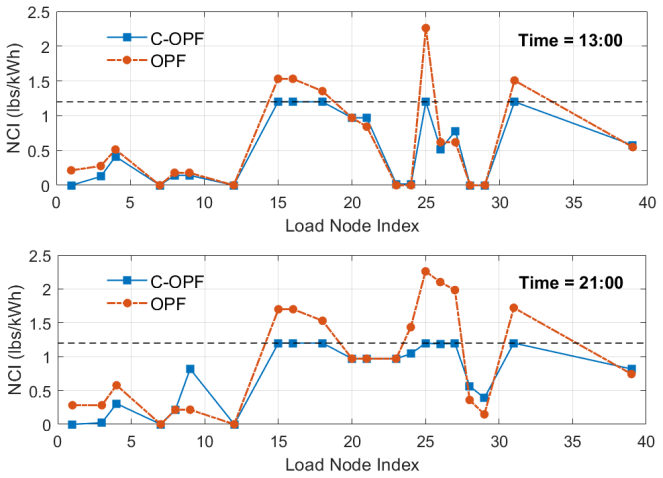

Fig. 6. The nodal carbon intensities (NCI) for all load nodes under the C-OPF-based and OPF-based economic dispatch schemes at 13:00 and 21:00. (The black dashed line denotes the NCI cap $\bar{w}_{i,t} = 1.2$ lbs/kWh).

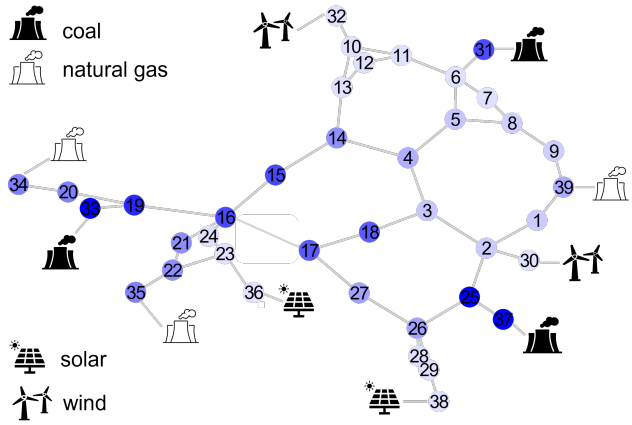

Fig. 7. Visualization of nodal carbon intensities of the modified New England 39-bus test system at 13:00. (Darker color indicates higher carbon intensity).

ED model that does not incorporate the carbon flow model and constraints. Essentially, the OPF-based ED model is a reduced version of the C-ED model (27), which excludes the carbon-related constraints (27p), (23), (24) and does not need the introduction of dual power flow variables. The OPF-based ED model is also a nonconvex optimization problem due to the full AC power flow equations and the dynamic ES power model, and we solve it using the solver IPOPT [44].

B. Test System and Simulation Settings

In the simulations, we consider day-ahead economic dispatch with $T = 12$ time steps and 2-hour time intervals. The modified New England 39-bus system, as shown in Figure 5, is used as the test system, which includes 3 coal power plants, 3 natural gas power plants, 2 wind farms, 2 solar farms, 3 ES systems, and 21 loads. The generation carbon emission factors $w^{\mathrm{G}}_{i,g}$ are 2.26, 0.97, and 0 (lbs/kWh) for coal plants, natural gas plants, and renewable generators, respectively. The carbon flow constraint (27p) is imposed for all the load nodes and all $t \in \mathcal{T}$, and we set the cap $\bar{w}_{i,t} = 1.2$ lbs/kWh.[3] For each ES system, we set the storage efficiency factor as $\kappa_i = 0.99$ and the charging and discharging efficiency coefficients as $\eta^{\mathrm{ch}}_i = \eta^{\mathrm{dc}}_i = 0.98$. Other detailed system parameters and settings are provided in [46].

C. Simulation Results Comparison of C-OPF and OPF

1) Nodal Carbon Intensity: Figure 6 illustrates the nodal carbon intensities for all load nodes under the C-OPF-based and OPF-based ED schemes, respectively. It shows that the C-OPF-based ED model can generate effective power dispatch schemes that keep the nodal carbon intensities of load nodes below the cap of $\bar{w}_{i,t} = 1.2$ lbs/kWh. In contrast, the OPF-based ED scheme frequently exceeds the nodal carbon intensity cap. Moreover, the grid's nodal carbon intensities exhibit significant temporal variation and spatial diversity. From Figure 6, it is observed that the nodal carbon intensities at 13:00 are generally lower than those at 21:00, due to the higher penetration of renewable generation at 13:00, as illustrated in Figure 8. Figure 7 visualizes the grid's nodal carbon intensities at 13:00, with darker blue colors indicating higher carbon intensity at each node. It demonstrates that the nodal carbon intensities calculated using the carbon flow method can reflect the proximity to different fuel types of generation and align with the physical power flow. In comparison, the grid average emission factor at 13:00 is calculated to be 0.5 lbs/kWh, which only gives an indication of the overall grid average emission state and falls short of providing detailed insight into local emissions at different locations.

2) Power Dispatch Scheduling Decisions: Figure 8 illustrates the generation decisions of the C-OPF-based and OPF-based ED schemes over a 24-hour period. In both schemes, the renewable generation, i.e., solar and wind generation, is fully utilized without curtailment. The primary distinction is that the C-OPF-based ED scheme results in more generation from expensive yet clean natural gas plants and less generation from cheap but high-emission coal plants to meet the carbon emission constraints, compared with the OPF scheme. The

[3] In the simulations, we set the same carbon intensity cap for all load nodes and all times for simplicity. In practical applications, distinct carbon intensity caps can be implemented for different nodes to distinguish the "cleanness" level of electricity supply at specific locations.

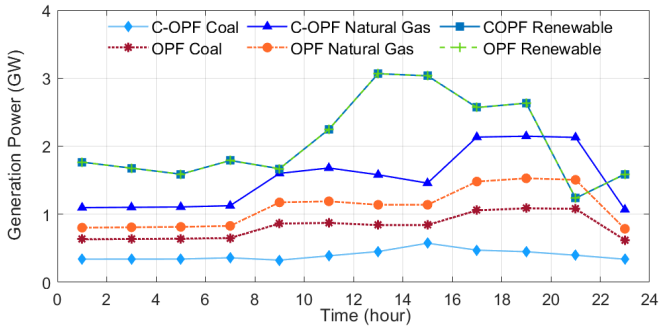

Fig. 8. The generation outputs of various power plants over 24 hours under the C-OPF-based and OPF-based economic dispatch schemes.

TABLE I
OPERATIONAL COST OF OPF-BASED AND C-OPF-BASED ED SCHEMES.

Cost (k$)	Coal	Natural Gas	Renewable	Energy Storage	Total
OPF	4515.4	6734.1	50.7	15.1	11315.3
C-OPF	1345.0	12116.3	50.7	15.7	13527.7

operational costs of these two ED schemes are presented in Table I. It is seen that the total operational cost of the C-OPF-based ED scheme is higher than that of the OPF scheme, due to the increased generation from natural gas plants as a substitute for coal plant generation.

3) Grid Carbon Emissions and Energy Storage: Figure 9 illustrates the total generation-side and attributed demand-side carbon emission rates over time. It is observed that the C-OPF-based ED scheme yields reduced carbon emission rates on both the generation side and demand side, compared with the OPF-based ED scheme. That is because the carbon flow constraint (27p) in the C-OPF model requires a larger share of power supply from clean generators to meet the nodal carbon intensity cap. As a result, the total system emissions over 24 hours are reduced from the amount of 69,981.9 klbs in the OPF scheme to 56,958.8 klbs in the C-OPF scheme.

Moreover, slight differences between the generation-side emission rates and the attributed load-side emission rates are observed in Figure 9 for both the OPF and C-OPF schemes. These differences result from the attributed emission rates for the operation of ES systems and power loss. Consistent with

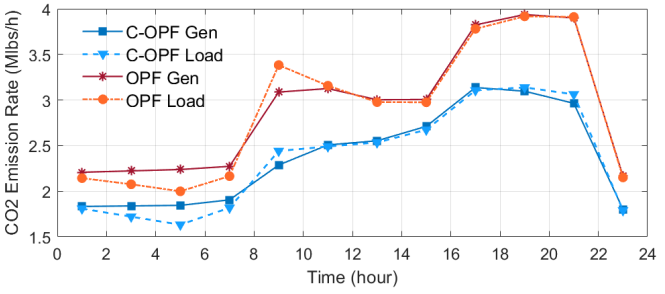

Fig. 9. The total (Scope 1) generation-side carbon emission rate and the total (Scope 2) attributed load-side carbon emission rate over time under the C-OPF-based and OPF-based economic dispatch schemes.

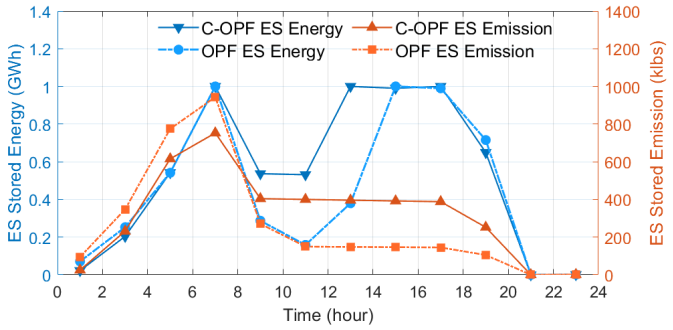

Fig. 10. The stored energy and virtual carbon emissions of the ES system at node-38 under the C-OPF-based and OPF-based economic dispatch schemes using the "water tank" ES carbon footprint model.

the power conservation law, our proposed carbon accounting mechanisms based on the carbon flow method ensure the "*carbon conservation principle*" [4] that the total generation-side carbon emissions equal the sum of emissions attributed to the total load, power loss, and ES systems at all times. Figure 10 illustrates the time trajectories of stored energy $e^{\text{es}}_{i,t}$ and virtual carbon emissions $E^{\text{es}}_{i,t}$ of the ES system at node-38. It is observed that the virtual carbon emissions generally increase when the ES system charges and decrease when it discharges. The period from 11:00 to 15:00, when charging does not result in increased emissions, occurs because the ES system charges with carbon-free renewable electricity. By combining Figures 9 and 10, it is seen that from 1:00 to 7:00, the generation-side emissions are higher than the load-side emissions due to the ES systems charging and absorbing emissions from the grid. Conversely, at 9:00, the ES systems are discharging and injecting emissions back into the grid, resulting in higher load-side emissions than the generation-side emissions.

Table II summarizes the carbon accounting results across 24 hours for the C-OPF-based and OPF-based ED schemes, where the (Scope 2) attributed emissions are calculated using the mechanisms introduced in Sections II-D and IV-A. It is verified that the total (Scope 1) generation-side emissions are equal to the total (Scope 2) emissions attributed to loads, grid power loss, and ES systems.

TABLE II
CARBON ACCOUNTING RESULTS BASED ON CARBON FLOW METHOD AND "WATER TANK" ES CARBON FOOTPRINT MODEL.

(klbs)	(Scope 1) Generation -Side Emissions	(Scope 2) Attributed Emissions		
		Load	Power Loss	ES Systems
OPF	69,982	69,273	639	70
C-OPF	56,959	56,433	457	69

D. Impact of Nodal Carbon Intensity Cap

To study the impact of the carbon flow constraint (27p), we adjust the nodal carbon intensity cap $\bar{w}_{i,t}$ from 1 lbs/kWh to 2.2 lbs/kWh uniformly for all load nodes, and run the C-OPF-based ED model for each case. Figure 11 illustrates the results of total system emissions and total operational costs under different carbon intensity caps. It is observed that as the nodal

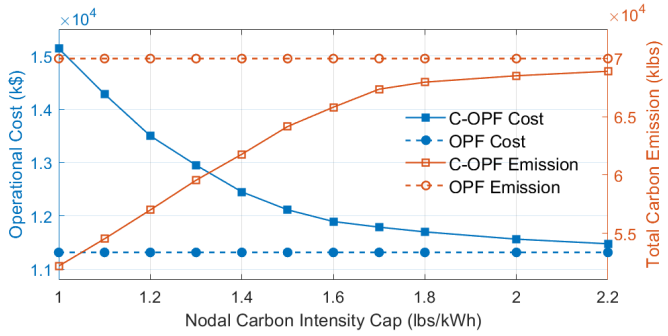

Fig. 11. Total system emissions and total operational costs of OPF-based and C-OPF-based ED schemes under different nodal carbon intensity caps $\bar{w}_{i,t}$.

carbon intensity cap increases, the total system operational cost of the C-OPF scheme decreases monotonically and converges to that of the OPF scheme; simultaneously, the total system carbon emissions increase and also converge to those of the OPF scheme. Essentially, the C-OPF-based ED scheme strikes an optimal trade-off between operational cost and carbon emission reduction. This is also consistent with the intuition that C-OPF solutions gradually reduce to traditional OPF solutions as carbon flow constraints become less restrictive.

E. Comparison of Two ES Carbon Footprint Models

In the simulations above, the "water tank" ES carbon footprint model is adopted in the C-OPF-based ED model and the carbon flow calculation for demand-side carbon accounting. In contrast, this subsection implements the "load/carbon-free generator (LCG)" ES carbon footprint model for comparison. The carbon accounting results using the LCG ES carbon footprint model are shown in Table III.

TABLE III
CARBON ACCOUNTING RESULTS BASED ON CARBON FLOW METHOD AND "LOAD/CARBON-FREE GENERATOR" ES CARBON FOOTPRINT MODEL.

(klbs)	(Scope 1) Generation -Side Emissions	(Scope 2) Attributed Emissions		
		Load	Power Loss	ES Systems
OPF	69,982	68,375	631	976
C-OPF	57,322	56,081	463	778

Compared with Table II that uses the "water tank" model, it is seen from Table III that for the OPF model, its optimal solution and generation-side emissions remain the same, as the OPF model does not involve carbon emissions. However, the attributed emissions calculated using the carbon flow method are different. Specifically, in the LCG ES carbon model, a greater share of the carbon footprints is attributed to the ES systems, thereby reducing the carbon footprints attributed to the loads and power loss. This is because, unlike the "water tank" model, ES systems are treated as pure loads during charging in the LCG model. As a result, virtual carbon emissions absorbed from the grid accumulate locally at the ES systems and are not released back to the grid during discharging, which become the carbon footprints of the ES systems. In terms of the C-OPF model, using the LCG ES carbon footprint model alters its optimal solution, leading to higher generation-side emissions and a reduced operational cost of $13,506.2$ k$. Because the ES systems impact the grid's carbon flow only during discharging, when the LCG ES carbon footprint model treats ES systems as carbon-free generators that lower the grid's carbon intensities. Thus, it allows for increased generation from high-emission but cheaper coal plants, while still satisfying the nodal carbon intensity constraints. Similarly, in the C-OPF case, much higher carbon footprints of 778 klbs are attributed to the ES systems, in contrast to the 69 klbs shown in Table II under the "water tank" model.

F. Computational Efficiency

The numerical experiments are implemented in a computing environment with Intel(R) Core(TM) i7-1185G7 CPUs running at 3.00 GHz and with 16 GB RAM. We use the JuMP language [47] in Julia to build optimization models and solve them using the IPOPT solver (version 3.14.10) [44]. It takes 176.6 seconds on average to solve the C-OPF-based ED model and 55.6 seconds to solve the OPF-based ED model.

Additionally, we implement the DC power flow model (11) instead of the full AC power flow model in the C-OPF-based and OPF-based ED models for simulation comparison. In this case, both ED models are significantly simplified due to omitting voltage magnitude and reactive power, neglecting power line losses, and replacing nonlinear power flow equations with linear DC flow equations. Under the DC power flow model, it takes 16.4 seconds on average to solve the C-OPF-based ED model and 1.2 seconds to solve the OPF-based ED model.

Due to the dual power flow reformulation and the addition of carbon flow equations and constraints, the C-OPF model generally has a larger problem size and requires more solution time than the traditional OPF model. In practice, several methods can improve the solution efficiency of the C-OPF model. For instance, by inspecting all branches and identifying those whose power flow directions can be predetermined based on the network configuration, the dual power flow reformulation can be avoided for these branches. Additionally, the solutions of the OPF model can be employed to warm-start the C-OPF model. A key future research direction is to develop efficient linearization and convexification approaches for the nonconvex carbon flow equations to fundamentally enhance the solution efficiency of the C-OPF model.

VI. CONCLUSION

This paper proposes a generic Carbon-aware Optimal Power Flow (C-OPF) methodology as a fundamental tool for guiding decarbonization decision-making in electric power systems. As a carbon-aware generalization of conventional OPF models, the C-OPF model enables the joint management of the grid's carbon footprints and power flows. A reformulation technique is introduced to address the issue of unknown power flow directions in the C-OPF model. Additionally, we propose two novel carbon footprint models for ES systems as well as their corresponding carbon accounting mechanisms, facilitating optimal carbon-aware ES operation. Numerical simulations

demonstrate that C-OPF-based schemes can effectively coordinate diverse energy resources for grid decarbonization while ensuring that decisions comply with regulatory requirements on carbon footprints. This paper represents preliminary work introducing the emerging and promising technique of C-OPF for supporting optimal power system decarbonization decisions. Extensive future research is anticipated to further advance the methodology of C-OPF. Potential future directions include 1) theoretical advances in the C-OPF modeling and optimization, such as efficient linearization and convexification of the C-OPF model, and 2) practical applications of C-OPF to power grid decision-making problems, such as carbon-aware demand response and carbon-electricity pricing.

APPENDIX A
DERIVATION OF CARBON FLOW MATRIX FORM (5)

From (4), we first multiply both sides by the denominator of (4) and move the term $\sum_{k\in\mathcal{N}_i^+} w_k P_{ki}^i$ to the left-hand side, leading to (28) for all $i \in \mathcal{N}$:

$$w_i \underbrace{\Big(\sum_{g\in\mathcal{G}_i} P_{i,g}^{\mathrm{G}} + \sum_{k\in\mathcal{N}_i^+} P_{ki}^i \Big)}_{:=P_i^{\mathrm{in}}} - \sum_{k\in\mathcal{N}_i^+} w_k P_{ki}^i = R_i^{\mathrm{G}}, \tag{28}$$

where $R_i^{\mathrm{G}} := \sum_{g\in\mathcal{G}_i} w_{i,g}^{\mathrm{G}} P_{i,g}^{\mathrm{G}}$ denotes the total generation carbon emission rate at node i. We then stack up equation (28) for all nodes $i \in \mathcal{N}$ into a column form. On the left-hand side, the first term of (28) becomes $\boldsymbol{P}_{\mathrm{N}}\boldsymbol{w}_{\mathrm{N}}$, where $\boldsymbol{w}_{\mathrm{N}} := (w_i)_{i\in\mathcal{N}}$ is the column vector that collects the nodal carbon intensities w_i, and $\boldsymbol{P}_{\mathrm{N}} := \mathrm{diag}(P_i^{\mathrm{in}})$ is the diagonal matrix whose i-th diagonal entry is the nodal active power inflow P_i^{in} to node i. The second term of (28) becomes $-\boldsymbol{P}_{\mathrm{B}}\boldsymbol{w}_{\mathrm{N}}$, where $\boldsymbol{P}_{\mathrm{B}} \in \mathbb{R}^{N\times N}$ is the branch power inflow matrix that is constructed by letting $\boldsymbol{P}_{\mathrm{B}}[i,k] = P_{ki}^i$ and $\boldsymbol{P}_{\mathrm{B}}[k,i] = 0$ if node k sends power flow P_{ki}^i to node i. The right-hand side of (28) becomes the column vector $\boldsymbol{r}_{\mathrm{G}} := (R_i^{\mathrm{G}})_{i\in\mathcal{N}}$. Thus, equation (28) for all $i \in \mathcal{N}$ can be equivalently reformulated as (29):

$$(\boldsymbol{P}_{\mathrm{N}} - \boldsymbol{P}_{\mathrm{B}})\boldsymbol{w}_{\mathrm{N}} = \boldsymbol{r}_{\mathrm{G}}. \tag{29}$$

Taking the matrix inverse of (29) leads to (5). See [14] for more derivation details.

REFERENCES

[1] Intergovernmental Panel on Climate Change (IPCC), "Climate change 2022: Impacts, adaptation and vulnerability," 2022.

[2] U.S. Energy Information Administration, "Monthly energy review: May 2023," 2023.

[3] World Resources Institute, "GHG protocol scope 2 guidance: An amendment to the GHG protocol corporate standard," 2015.

[4] X. Chen, H. Chao, W. Shi, and N. Li, "Towards carbon-free electricity: A flow-based framework for power grid carbon accounting and decarbonization," *accepted to IET Energy Convers. Econ.*, 2024.

[5] World Resources Institute, "The greenhouse gas protocol: A corporate accounting and reporting standard," 2004.

[6] L. F. Valenzuela, A. Degleris, A. E. Gamal, M. Pavone, and R. Rajagopal, "Dynamic locational marginal emissions via implicit differentiation," *IEEE Transactions on Power Systems*, vol. 39, no. 1, pp. 1138–1147, 2024.

[7] Kevala Inc., "Total carbon accounting: A framework to deliver locational carbon intensity data," Nov. 2021. [Online]. Available: https://www.kevala.com/resources/total-carbon-accounting

[8] M. Brander, M. Gillenwater, and F. Ascui, "Creative accounting: A critical perspective on the market-based method for reporting purchased electricity (scope 2) emissions," *Energy Policy*, vol. 112, pp. 29–33, Jan. 2018.

[9] C. Lau and J. Aga, "Bottom line on renewable energy certificates," 2008. [Online]. Available: https://www.wri.org/research/bottom-line-renewable-energy-certificates

[10] R. Kansal, "Introduction to the virtual power purchase agreement," *Rocky Mountain Institute*, Nov. 2018.

[11] G. J. Miller, K. Novan, and A. Jenn, "Hourly accounting of carbon emissions from electricity consumption," *Environ. Res. Lett.*, vol. 17, no. 4, p. 044073, Apr. 2022.

[12] The Electric Power Research Institute (EPRI), "24/7 carbon-free energy: Matching carbon-free energy procurement to hourly electric load," Dec. 2022.

[13] C. Kang, T. Zhou, Q. Chen, Q. Xu, Q. Xia, and Z. Ji, "Carbon emission flow in networks," *Scientific Reports*, vol. 2, no. 1, p. 479, Jun. 2012.

[14] C. Kang, T. Zhou, Q. Chen, J. Wang, Y. Sun, Q. Xia, and H. Yan, "Carbon emission flow from generation to demand: A network-based model," *IEEE Trans. Smart Grid*, vol. 6, no. 5, pp. 2386–2394, Sept. 2015.

[15] B. Li, Y. Song, and Z. Hu, "Carbon flow tracing method for assessment of demand side carbon emissions obligation," *IEEE Trans. Sustain. Energy*, vol. 4, no. 4, pp. 1100–1107, Oct. 2013.

[16] Y. Chen, D. Deka, and Y. Shi, "Contributions of individual generators to nodal carbon emissions," in *Proceedings of the 15th ACM International Conference on Future and Sustainable Energy Systems*, 2024, pp. 415–421.

[17] J. Bialek, "Tracing the flow of electricity," *IEE Proceedings-Generation, Transmission and Distribution*, vol. 143, no. 4, pp. 313–320, 1996.

[18] S. Frank, I. Steponavice, and S. Rebennack, "Optimal power flow: a bibliographic survey I: Formulations and deterministic methods," *Energy Systems*, vol. 3, no. 3, pp. 221–258, Apr. 2012.

[19] M. B. Cain, R. P. O'neill, A. Castillo *et al.*, "History of optimal power flow and formulations," *Federal Energy Regulatory Commission*, vol. 1, pp. 1–36, Dec. 2012.

[20] X. Chen, E. Dall'Anese, C. Zhao, and N. Li, "Aggregate power flexibility in unbalanced distribution systems," *IEEE Trans. Smart Grid*, vol. 11, no. 1, pp. 258–269, Jan. 2020.

[21] X. Chen, C. Zhao, and N. Li, "Distributed automatic load frequency control with optimality in power systems," *IEEE Control Netw. Syst.*, vol. 8, no. 1, pp. 307–318, Mar. 2021.

[22] X. Chen, W. Wu, and B. Zhang, "Robust capacity assessment of distributed generation in unbalanced distribution networks incorporating anm techniques," *IEEE Trans. Sustain. Energy*, vol. 9, no. 2, pp. 651–663, Apr. 2018.

[23] Y. Sun, C. Kang, Q. Xia, Q. Chen, N. Zhang, and Y. Cheng, "Analysis of transmission expansion planning considering consumption-based carbon emission accounting," *Applied Energy*, vol. 193, pp. 232–242, May 2017.

[24] W. Shen, J. Qiu, K. Meng, X. Chen, and Z. Y. Dong, "Low-carbon electricity network transition considering retirement of aging coal generators," *IEEE Trans. Power Syst.*, vol. 35, no. 6, pp. 4193–4205, Nov. 2020.

[25] Y. Cheng, N. Zhang, and C. Kang, "Bi-level expansion planning of multiple energy systems under carbon emission constraints," in *Proc. of IEEE PES General Meeting*. IEEE, 2018, pp. 1–5.

[26] T. Wu, X. Wei, X. Zhang, G. Wang, J. Qiu, and S. Xia, "Carbon-oriented expansion planning of integrated electricity-natural gas systems with EV fast-charging stations," *IEEE Trans. Transp. Electr.*, vol. 8, no. 2, pp. 2797–2809, Jun. 2022.

[27] X. Wei, K. W. Chan, T. Wu, G. Wang, X. Zhang, and J. Liu, "Wasserstein distance-based expansion planning for integrated energy system considering hydrogen fuel cell vehicles," *Energy*, vol. 272, p. 127011, Jun. 2023.

[28] C. Gu, Y. Liu, J. Wang, Q. Li, and L. Wu, "Carbon-oriented planning of distributed generation and energy storage assets in power distribution network with hydrogen-based microgrids," *IEEE Trans. Sustain. Energy*, vol. 14, no. 2, pp. 790–802, Apr. 2023.

[29] Y. Wang, J. Qiu, and Y. Tao, "Optimal power scheduling using data-driven carbon emission flow modelling for carbon intensity control," *IEEE Trans. Power Syst.*, vol. 37, no. 4, pp. 2894–2905, Jul. 2021.

[30] L. Sang, Y. Xu, and H. Sun, "Encoding carbon emission flow in energy management: A compact constraint learning approach," *IEEE Trans. Sustain. Energy*, vol. 15, no. 1, pp. 123–135, Jan. 2024.

[31] Y. Wang, J. Qiu, and Y. Tao, "Robust energy systems scheduling considering uncertainties and demand side emission impacts," *Energy*, vol. 239, p. 122317, Jan. 2022.

[32] Z. Lu, L. Bai, J. Wang, J. Wei, Y. Xiao, and Y. Chen, "Peer-to-peer joint electricity and carbon trading based on carbon-aware distribution locational marginal pricing," *IEEE Trans. Power Syst.*, vol. 38, no. 1, pp. 835–852, Jan. 2023.
[33] Y. Cheng, N. Zhang, B. Zhang, C. Kang, W. Xi, and M. Feng, "Low-carbon operation of multiple energy systems based on energy-carbon integrated prices," *IEEE Trans. Smart Grid*, vol. 11, no. 2, pp. 1307–1318, Mar. 2020.
[34] Washington Department of Commerce, "Energy storage accounting issues," 2021.
[35] Federal Energy Regulatory Commission, "Accounting and reporting treatment of certain renewable energy assets," 2022.
[36] Y. Gu, J. Li, X. Xing, Z. Cai, G. Deng, T. Sun, and Z. Li, "Carbon emission flow calculation of power systems considering energy storage equipment," in *Proc. of 8th Asia Conference on Power and Electrical Engineering*. IEEE, 2023, pp. 1268–1272.
[37] X. Chen, "Enhance low-carbon power system operation via carbon-aware demand response," *Energy Internet*, p. e12004, Oct. 2024.
[38] G. H. Golub and C. F. Van Loan, *Matrix computations*. The Johns Hopkins University Press, 2013.
[39] P. Shivakumar and K. H. Chew, "A sufficient condition for nonvanishing of determinants," *Proceedings of the American Mathematical Society*, pp. 63–66, 1974.
[40] T. Ando, "Inequalities for M-matrices," *Linear and Multilinear Algebra*, vol. 8, no. 4, pp. 291–316, 1980.
[41] A. Lorca and X. A. Sun, "Adaptive robust optimization with dynamic uncertainty sets for multi-period economic dispatch under significant wind," *IEEE Trans. Power Syst.*, vol. 30, no. 4, pp. 1702–1713, Jul. 2015.
[42] G. B. Giannakis, V. Kekatos, N. Gatsis, S. Kim, H. Zhu, and B. F. Wollenberg, "Monitoring and optimization for power grids: A signal processing perspective," *IEEE Signal Process. Mag.*, vol. 30, no. 5, pp. 107–128, Sept. 2013.
[43] R. Fletcher and S. Leyffer, "Solving mathematical programs with complementarity constraints as nonlinear programs," *Optimiz. Methods and Soft.*, vol. 19, no. 1, pp. 15–40, 2004.
[44] L. T. Biegler and V. M. Zavala, "Large-scale nonlinear programming using IPOPT: An integrating framework for enterprise-wide dynamic optimization," *Comput. & Chemic. Engine.*, vol. 33, no. 3, pp. 575–582, Mar. 2009.
[45] X. Chen and N. Li, "Leveraging two-stage adaptive robust optimization for power flexibility aggregation," *IEEE Trans. Smart Grid*, vol. 12, no. 5, pp. 3954–3965, Mar. 2021.
[46] X. Chen, "Configuration and parameters of modified 39-bus New England test system," 2023. [Online]. Available: https://xchen.engr.tamu.edu/wp-content/uploads/sites/294/2024/01/39system.pdf
[47] M. Lubin, O. Dowson, J. Dias Garcia, J. Huchette, B. Legat, and J. P. Vielma, "JuMP 1.0: Recent improvements to a modeling language for mathematical optimization," *Math. Program. Comput.*, 2023.

Xin Chen is an Assistant Professor in the Department of Electrical and Computer Engineering at Texas A&M University (TAMU). Dr. Chen directs the Smart Power, Energy and Decision-making (SPEED) Lab at TAMU. His research lies in the intersection of control, machine/reinforcement learning, and optimization for smart sustainable power and energy systems. He received the Ph.D. degree in electrical engineering from Harvard University, the master's degree in electrical engineering and two bachelor's degrees in engineering and economics from Tsinghua University. He was a Postdoctoral Associate affiliated with MIT Energy Initiative at Massachusetts Institute of Technology. He is a recipient of the IEEE PES Outstanding Doctoral Dissertation Award, IEEE Transactions on Smart Grid Top-5 Outstanding Papers, and multiple best paper awards at IEEE control and power conferences.

Andy Sun is is the Iberdrola-Avangrid Professor in Electric Power Systems in the Sloan School of Management at the Massachusetts Institute of Technology (MIT). He received his PhD degree in Operations Research from MIT and was a postdoctoral fellow in the Mathematical Sciences division of the IBM T. J. Watson Research Center at Yorktown Heights, NY. He was a faculty member in the School of Industrial and Systems Engineering at Georgia Institute of Technology before joining MIT. Dr. Sun's research focuses on optimization and computation for large-scale electric power system control, operations, and planning, market design for power grid decarbonization, and electrification of transportation. His research on robust operation of power grids has been influential in improving reliability unit commitment in ISO/RTO markets.

Wenbo Shi is the Founder/CEO of Singularity Energy, a startup that offers advanced carbon and clean energy management software and data solutions for utilities, grid operators, corporations and technology providers to accurately measure emissions and optimize their decision-making for grid decarbonization. Singularity is proud to partner with organizations such as Southern Company, MISO, Eversource Energy, Enersponse, Sense, and Measurable.Before founding Singularity, Wenbo was a postdoctoral researcher at Harvard University. He received his Ph.D. from University of California, Los Angeles in 2015.

Na Li is a Winokur Family Professor of Electrical Engineering and Applied Mathematics at Harvard University. She received her Bachelor's degree in Mathematics from Zhejiang University in 2007 and Ph.D. degree in Control and Dynamical systems from California Institute of Technology in 2013. She was a postdoctoral associate at the Massachusetts Institute of Technology 2013-2014. She has held a variety of short-term visiting appointments including the Simons Institute for the Theory of Computing, MIT, Google Brain, and MERL. Her research lies in the control, learning, and optimization of networked systems, including theory development, algorithm design, and applications to real-world cyber-physical societal system.

Carbon-Aware Optimal Power Flow with Data-Driven Carbon Emission Tracing

Zhentong Shao
University of California Riverside
Riverside, CA, USA
Email: zhentons@ucr.edu

Nanpeng Yu
University of California Riverside
Riverside, CA, USA
Email: nyu@ece.ucr.edu

***Abstract*—Quantifying locational carbon emissions in power grids is crucial for implementing effective carbon reduction strategies for customers relying on electricity. This paper presents a carbon-aware optimal power flow (OPF) framework that incorporates data-driven carbon tracing, enabling rapid estimation of nodal carbon emissions from electric loads. By developing generator-to-load carbon emission distribution factors through data-driven technique, the analytical formulas for both average and marginal carbon emissions can be derived and integrated seamlessly into DC OPF models as linear constraints. The proposed carbon-aware OPF model enables market operators to optimize energy dispatch while reducing greenhouse gas emissions. Simulations on IEEE test systems confirm the accuracy and computational efficiency of the proposed approach, highlighting its applicability for real-time carbon-aware system operations.**

I. Introduction

The decarbonization of power systems is a top priority to combat climate change. In 2023, the U.S. electric power sector emitted 1,427 million metric tons of CO_2, accounting for over 29.7% of the nation's total energy-related emissions [1]. Effective grid decarbonization relies on accurate measurement of carbon emissions associated with both electricity production and consumption, commonly referred to as carbon tracing. This process quantifies emissions, providing a useful signal for decisions related to decarbonization strategies. Since the demand for electricity drives fossil fuel consumption from power generation stations, it is essential to calculate not only carbon emission from generation but also end-user carbon footprints by attributing generation-based emissions to consumers in proportion to their electricity usage.

Existing literature explores various methods for quantifying carbon emissions within power grids, emphasizing the need for tools that measure emissions at the nodal level to guide effective carbon reduction practices. Traditional methods for calculating system-level carbon emissions across all generators without considering geographical or load-specific variations. Virtual carbon flow models [2] have emerged to track carbon transfers between regions, while statistical [3], [4] and machine learning [5] forecasting models utilize factors like weather and load to predict network or region-wide emissions. However, they fail to provide location-specific insights.

Recent research has focused on developing tools for nodal emission calculations to support real-time operation by grid operators [6]. Two key metrics are nodal average carbon emissions, which reflect the overall carbon intensity of power consumption, and nodal marginal carbon emissions, which measure increase in overall carbon emission due to incremental load changes. Specifically, reference [7] establishes an incremental optimal power flow (OPF) model to evaluate the marginal carbon emissions for a given power flow scenario. Reference [8] quantifies the changes in system-wide carbon emissions resulting from the activation of local demand response resource. Reference [9] implements a load control strategy that uses a lookup table to evaluate nodal marginal carbon emissions. Reference [10] proposes a load-shifting algorithm with an incremental OPF model to capture the marginal carbon emissions of data centers. These methods typically require solving an incremental OPF near a specified operating point to capture locational carbon emissions, yet solving an integrated system optimization problem with carbon awareness remains challenging.

Analytical methods using carbon emission flow have also been explored. Reference [11] established carbon emission flow equations and employed iterative algorithms to trace carbon emissions back to specific generators, though the solution lacks convergence guarantees, limiting its practical application. Reference [12] calculates the nodal power flow mix through analytical derivations and employs matrix inversion to map carbon emissions from generators to demands. However, the invertibility of the matrix cannot be guaranteed in the presence of loop flows and bilateral contracts. More recent innovations address these limitations by directly linking generator emissions to individual nodal loads using computationally efficient depth-first search algorithms [13], which calculate both average and marginal carbon emissions. However, this approach serves primarily as an evaluation tool for given system states and is challenging to integrate into an OPF problem. To address this, [14] introduces a carbon-aware OPF model with nonlinear carbon flow equations, offering a promising carbon accounting tool for economic dispatch, though its non-convex formulation significantly increases computational costs.

In response to the limitations of existing studies, this paper presents a data-driven method to determine both the average nodal carbon emission (ANCE) rate and the locational marginal carbon emission (LMCE) rate. Given that carbon flow is physically coupled with power flow, we trained an affine mapping to trace power flows from individual generators

to nodal loads, which are called generator-to-load distribution factors. Using these factors, the analytical forms of ANCE and LMCE are derived. The resulting carbon emission quantification tool is linear, making it straightforward to integrate into optimal power flow models. Accordingly, this paper proposes a carbon-aware OPF model based on the data-driven carbon tracing approach. The proposed method is verified using several IEEE test systems. The test results demonstrated the effectiveness of the proposed method.

II. Methodology

A. Tracing Nodal Carbon Emission

Consider a power network with N nodes and L transmission lines. Let $\mathcal{N}$ denote the set of all nodes, $\mathcal{L}$ the set of lines, and $\mathcal{G}$ the set of generators. At each time period, d_n represents the load demand at node n. For a node without load, $d_n = 0$. The system operator solves the OPF problem to determine the power dispatch p_g for G generators. Each generator g has a carbon emission rate γ_g, expressed in units of lbs CO_2/MWh. The goal of this paper is to model carbon emissions in the OPF framework and calculate the nodal carbon emission e_n attributed to the loads at each node n.

The carbon emissions in a power system are created by the generators and subsequently allocated to the electric loads. The power consumed is not inherently tied to any specific generator. To facilitate carbon tracing, we assume the power flow is divisible and it follows a consistent allocation rule. This is formally stated in Assumption 1, which enables a proportional division of power flow.

Assumption 1. *For any node n, the proportion of power inflow attributable to generator g is equal to the proportion of the power outflow attributable to generator g.*

Assumption 1 implies that generators' contributions are proportionally allocated across the network, ensuring consistency in carbon tracing of power flows. Under Assumption 1, the contribution of each generator g to the nodal load n is denoted as $d_{n,g}$, and the nodal carbon emission e_n is computed using (1), where $F_{g\to n}(\cdot)$ denotes the mapping used to calculate the contribution of generator g to load n.

$$d_{n,g} = F_{g\to n}(p_g) \tag{1a}$$

$$e_n = \sum_{g=1}^{G} \gamma_g \, d_{n,g} \tag{1b}$$

By introducing the nodal carbon emission, we can incorporate carbon-aware constraints into the OPF problem, as shown in (2), where $e_{n,t}$ denotes the carbon emission of node n on time period t. Also, the nodal average carbon emission rate δ_n can be computed using (3).

$$\sum_{t=1}^{T} e_{n,t} \le E_n^{\max} \tag{2}$$

$$\delta_n = e_n / d_n \tag{3}$$

B. Data-Driven Estimation of Nodal Carbon Emission

It is shown in (1) that the key to calculating the nodal carbon emission is determining the specific form of the generator-to-load function $F_{g\to n}(\cdot)$. In fact, existing literature has investigated formulations for $F_{g\to n}(\cdot)$. For instance, reference [14] utilizes a non-convex mapping known as carbon flow equations, while [13] proposes a tree search algorithm based on a given flow result to determine the generator-to-load allocation. These studies indicate that there exist an approximately linear mapping between p_g and d_n. In this paper, we assume this mapping to be affine and employ a data-driven approach to determine it. Compared to existing methods, the proposed carbon tracing formula can be seamlessly integrated into the OPF framework as linear constraints, maintaining the computational efficiency of the OPF model and enabling a carbon-aware OPF solution.

We define the generator-to-load contribution mapping $F_{g\to d}(\cdot)$ with an affine formulation, given by $d_{n,g} = \alpha_{n,g}\, p_g$, where $\alpha_{n,g} \in [0,1]$ represents the generator-to-load contribution factor of generator g to the nodal load n. The total carbon emission of node n can then be estimated as:

$$e_n = \sum_{g=1}^{G} \alpha_{n,g}\gamma_g p_g \tag{4}$$

Here, the term $\alpha_{n,g}\gamma_g$ is referred to as the carbon emission distribution factor. The carbon emission rate γ_g is given for each generator g. Our objective is to determine $\alpha_{n,g}$ through data-driven techniques. To ensure the physical relevance of the data-driven results, we adopt Assumption 2. Assumption 2 essentially represents a lossless scenario, where all generated power is ultimately allocated to the nodal loads.

Assumption 2. *Under a lossless DC power flow model, the generator-to-load distribution factors satisfy: $\sum_{n=1}^{N} \alpha_{n,g} = 1, \forall g \in \mathcal{G}$.*

A constrained regression problem is defined to determine $\alpha_{n,g}$. Given the power flow set $\mathcal{S}$, (5) can be solved for each generator to obtain the generator-to-load distribution factors.

$$\min_{\alpha_{n,g}} \; J_g = \sum_{s=1}^{S} \left(d_n^{(s)} - \alpha_{n,g} p_g^{(s)} \right)^2 \tag{5a}$$

$$\text{s.t.} \sum_{n=1}^{N} \alpha_{n,g} = 1 \tag{5b}$$

(5) is a convex non-linear programming problem, which can be efficiently tackled by the commercial solvers like Gurobi.

C. Locational Marginal Carbon Emission

After obtaining the factors $\alpha_{n,g}$, we can express nodal demand in terms of generator output using (6). By combining (4) and (6), we can derive the locational marginal carbon emission rate for each node.

$$d_n = \sum_{g=1}^{G} \alpha_{n,g} p_g. \tag{6}$$

Let μ_n denote the LMCE rate at node n, which can be calculated using (7).

$$\mu_n = \frac{\partial e_n}{\partial d_n}. \tag{7}$$

The closed form solution for the LMCE rate is shown in (8). Details of the derivation for (8) are provided in Appendix A.

$$\mu_n = \frac{\partial e_n}{\partial d_n} = \frac{\sum_{g=1}^{G} \alpha_{n,g}^2 \gamma_g}{\sum_{g=1}^{G} \alpha_{n,g}^2}. \tag{8}$$

The LMCE rate μ_n can be interpreted as the weighted carbon emission rate of generators γ_g, with weighting factors $\alpha_{n,g}^2$. Since the generator-to-load distribution factor $\alpha_{n,g}$ is computed through a data-driven method, μ_n is referred to as the data-driven LMCE rate.

Remark 1. *The data-driven LMCE rate (8) acts as a tool to approximate the actual carbon emissions. The power flow scenario considered for the LMCE should be adequately represented by the power flow scenarios in the training dataset. In practical applications, (8) should be adjusted to (9), where $\mathcal{G}^*$ represents the set of generators in service within the evaluated power flow scenario.*

$$\mu_n = \frac{\partial e_n}{\partial d_n} = \frac{\sum_{g\in\mathcal{G}^*} \alpha_{n,g}^2 \gamma_g}{\sum_{g\in\mathcal{G}^*} \alpha_{n,g}^2} \tag{9}$$

D. Carbon-Aware OPF with Carbon Distribution Factors

This subsection incorporates data-driven carbon emission distribution factors into the OPF problem, keeping it as an efficient linear programming (LP) problem with carbon-aware OPF solutions. The resulting carbon-aware OPF model is presented in (10).

$$\min_{p_g, e_n} f_{\text{power}}(p_g, \forall g) + f_{\text{carbon}}(p_g, \forall g) \tag{10a}$$

$$\text{s.t.} \sum\nolimits_{g\in\mathcal{G}} p_g - \sum\nolimits_{n\in\mathcal{N}} d_n = 0 \tag{10b}$$

$$p_l = \Gamma_{l,n} \left(\sum\nolimits_{g\in\mathcal{G}(n)} p_g - d_n \right), \ \forall l \in \mathcal{L} \tag{10c}$$

$$-P_l^{\max} \le p_l \le P_l^{\max}, \ \forall l \in \mathcal{L} \tag{10d}$$

$$P_g^{\min} \le p_g \le P_g^{\max}, \ \forall g \in \mathcal{G} \tag{10e}$$

$$e_n = \sum\nolimits_{g\in\mathcal{G}} \alpha_{n,g}\gamma_g p_g, \ \forall n \in \mathcal{N} \tag{10f}$$

$$\sum\nolimits_{n\in\mathcal{N}} e_n \le E_{\text{total}} \tag{10g}$$

The objective (10a) minimizes the overall cost, which includes the power-related cost f_{power} and the carbon emission-related cost f_{carbon}. Depending on the specific application, f_{power} may represent generation costs, network losses and etc. The term f_{carbon} is is defined to capture the equivalent costs for carbon emissions associated with either the generation or demand side, such as carbon emission permit fees for generators. A sample cost function is provided in (11).

$$f_{\text{power}} := \sum\nolimits_{g\in\mathcal{G}} \left(a_g p_g^2 + b_g p_g + c_g \right), \tag{11a}$$

$$f_{\text{carbon}} := c^{\text{emp}} \sum\nolimits_{g\in\mathcal{G}} \gamma_g p_g, \tag{11b}$$

where (11a) denotes the total generation cost in quadratic form with parameters a_g, b_g, and c_g, and (11b) denotes the carbon emission cost for generators with permit price c^{emp}.

(10b) represents the system-wide power balance constraint under a lossless DC power flow model. (10c) calculates line power flows using the power transfer distribution factors $\Gamma_{l,n}$, where $\mathcal{G}(n)$ denotes the set of generators located at node n. Constraints (10d) limit the allowable range for line power flows, while constraints (10e) enforce the capacity limits for generators. (10f) calculates nodal carbon emissions based on data-driven carbon emission distribution factors, and (10g) regulates the allowable system-level carbon emission. (10g) provides a basic carbon constraint for illustration purposes. With (10f), various customized carbon constraints can be developed as those in reference [14].

The proposed carbon-aware OPF framework (10) has a computationally efficient LP structure, allowing direct extension to a multi-period dispatch model or integration into the unit commitment problem. This formulation provides a carbon-aware generalization of the DC-OPF model and can be efficiently solved through linear programming solvers such as CPLEX and Gurobi.

III. Case Study

The proposed carbon-aware OPF is evaluated on several IEEE test systems, including the 5-bus, 24-bus, 30-bus, and 118-bus system from MATPOWER 7.1 [15]. Numerical simulations are conducted based on the DC-OPF solver in MATPOWER. Load demands are adjusted according to a uniform distribution within the range [0.7, 1], and sample generation follows the method specified in [16]. Each test system is accompanied by 1,000 data samples, with 80% of the samples randomly selected as the training dataset and the remaining 20% as the testing dataset. Generators are assumed to be powered by fossil fuels, with carbon emission rates γ_g ranging from 113 to 2,388 lbs CO_2/MWh. The specific settings for generator carbon emissions can be found in [13].

A. Data-driven Generator-to-load Distribution Factors

The generator-to-load distribution factors, $\alpha_{n,g}$, are fundamental for calculating nodal carbon emissions. In this subsection, we estimate the data-driven generator-to-load distribution factors $\alpha_{n,g}$ and present the load approximation errors using the estimated $\alpha_{n,g}$ and generator outputs in Table I. The accuracy metrics include the mean absolute error (MAE) and maximum absolute error (Max-AE), both measured in megawatts (MW). As shown in Table I, the trained model demonstrates minimal load approximation errors, with an average MAE of 6.64×10^{-7} MW and a Max-AE of 2.81×10^{-5} MW. These results indicate that $\alpha_{n,g}$ effectively distributes generator output to meet load demands, which is crucial for accurate carbon tracing. The data also reveals a correlation between accuracy and system size: the highest Max-AE occurs in the 118-bus system, while the 5-bus system shows near-perfect result, with negligible error. This suggests that system complexity may impact the distribution factor's precision, with smaller systems exhibiting more accurate results.

TABLE I
ERROR OF LOAD DEMANDS APPROXIMATED BY DATA-DRIVEN GENERATOR-TO-LOAD FACTORS

Systems	**MAE (MW)**	**Max-AE (MW)**
5-bus	3.81×10^{-9}	1.12×10^{-8}
24-bus	2.37×10^{-6}	2.58×10^{-5}
30-bus	1.30×10^{-8}	1.23×10^{-6}
118-bus	2.68×10^{-7}	8.53×10^{-5}
Tol. Avg.	6.64×10^{-7}	2.81×10^{-5}

TABLE II
DATA-DRIVEN GENERATOR-TO-LOAD FACTORS OF THE 5-BUS SYSTEM

Indices	G-1	G-2	G-3
Bus-1	0	0	0
Bus-2	0.3154	0.2931	0.3021
Bus-3	0.2775	0.3099	0.2979
Bus-4	0.4071	0.3970	0.4000
Bus-5	0	0	0

The trained generator-to-load distribution factors for the 5-bus system are examined in detail. This system includes three generators located at buses 1, 3, and 5. As shown in Table II, generators G-1, G-2, and G-3 supply the loads at buses 2, 3, and 4, using distribution factors that reflect the load-sharing dynamics among generators. Notably, bus-4 receives the highest contributions from all generators, with distribution factors around 0.4, indicating a balanced load-sharing across the generators. In contrast, buses 2 and 3 exhibit greater variability, with slightly lower impacts from G-2 at Bus-2 and G-1 at Bus-3, respectively. Buses 1 and 5 do not serve load and thus has zero generator-to-load factors. This data-driven analysis highlights the spatio distribution of generator-to-load distribution factors across the network.

B. Data-driven Locational Marginal Carbon Emission Rate

In this subsection, we use (8) to calculate the LMCE rate, μ_n for a 30-bus system with 6 generators and settings of γ_g detailed in Table III. The resulting data-driven LMCE rates, μ_n, are shown in Fig. 1, alongside benchmark values derived from sensitivity analysis [6], [13] for each node. The node indices in Fig. 1 are sorted by μ_n values. From the test results in Fig. 1, it is evident that the calculated LMCE rates μ_n for the 30-bus system closely align with the benchmark values, demonstrating high accuracy. This data-driven approach effectively captures emission variations across the network, facilitating effective customer level carbon reduction in the power system.

TABLE III
CARBON EMISSION RATE OF GENERATORS IN THE 30-BUS SYSTEM

Gen. Index	G-1	G-2	G-3	G-4	G-5	G-6
γ_g (lbs CO_2/MWh)	565	1890	1145	1446	644	961

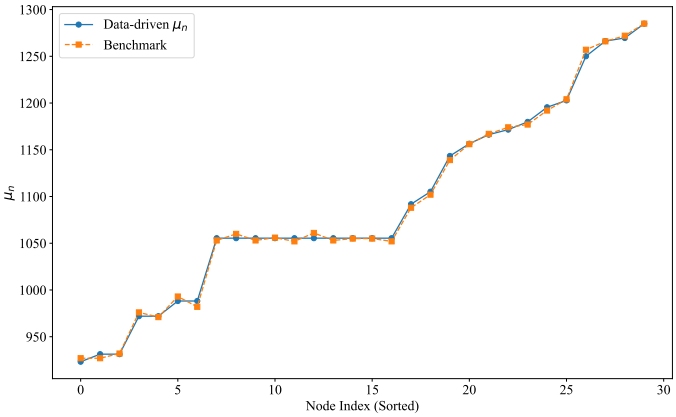

Fig. 1. The locational marginal carbon emission of the 30-bus system (with the indices on the x-axis sorted by the values of μ_n).

TABLE IV
PERFORMANCE OF THE CARBON-AWARE OPF ON 30-BUS SYSTEM

Metric	Baseline-OPF	Carbon-OPF
Power Cost ($)	3.58×10^3	3.70×10^3
Carbon Emission Cost ($)	1.82×10^3	1.71×10^3
Total Cost ($)	5.40×10^3	5.41×10^3
Total Emission (CO_2)	101.5 ton	95 ton
Solution Time (s)	0.082	0.089

C. Evaluation of Carbon-Aware OPF

In this subsection, the performance of the proposed carbon-aware OPF problem (10) with objective function (11) is evaluated. We define the OPF problem (10)-(11) without carbon constraints (10f)-(10g) as the baseline-OPF problem, while the version incorporating carbon constraints represents the proposed carbon-aware OPF. The parameter c^{emp} is set as 0.009$/lbs CO_2. The carbon-aware OPF includes a carbon constraints with $E_{\text{total}} = 95$ ton CO_2.

The results of the two OPF problems on the 30-bus system are presented in Table IV. As shown in Table IV, by introducing the carbon emission constraint, the carbon-aware OPF successfully identifies a generator dispatch scheme with reduced emissions, lowering emitted CO_2 from 101.5 tons to 95 tons. This reduction led to a slightly increased generation cost, from $\$3.58 \times 10^3$ to $\$3.70 \times 10^3$. The carbon-aware approach also results in a decrease in carbon emission cost, from $\$1.82 \times 10^3$ to $\$1.71 \times 10^3$, partially offsetting the higher power cost. Consequently, the total operational cost remains nearly unchanged, with only 0.19% or $10 increase in total cost. The OPF solution time experiences a slight increase from 0.082 to 0.089 seconds, indicating that the proposed method maintains computational efficiency. The carbon-aware OPF achieves a significant reduction in emissions with minimal cost impact, demonstrating the effectiveness of emission constraints in aligning power dispatch with environmental objectives while maintaining cost stability.

IV. Conclusion

This paper developed a data-driven approach to formulate and solve carbon-aware OPF problem, providing valuable locational marginal carbon emission rate signals to end-use customers to effectively reduce their carbon footprint. By estimating generator-to-load distribution factors, the proposed method enables the derivation of closed-form solution for both average and marginal nodal carbon emission rates. The integration of generator-to-load distribution factors into the OPF framework yields carbon-aware energy resource dispatch decisions, balancing power system operation cost and emissions reduction objectives. Simulation results on IEEE test systems demonstrate that the proposed method achieves significant emissions reductions with minimal impact on total operational costs, while maintaining computational efficiency. The proposed method serves as a valuable tool for supporting real-time carbon accounting and facilitating carbon-oriented demand management. Future work will focus on extending the model to incorporate multi-period and stochastic OPF scenarios, further enhancing its applicability to dynamically changing and uncertain grid conditions.

Appendix

A. Derivation of Locational Marginal Carbon Emission

Applying the chain rule to (4), we have:

$$\frac{\partial e_n}{\partial d_n} = \sum_{g=1}^{G} \left(\frac{\partial e_n}{\partial p_g} \cdot \frac{\partial p_g}{\partial d_n} \right) \tag{12}$$

Since d_n is a function of p_g, we need to find $\frac{\partial p_g}{\partial d_n}$. However, directly computing $\frac{\partial p_g}{\partial d_n}$ is difficult because d_n depends on all p_g. Instead, we can consider the relationship between e_n and d_n via their gradients with respect to p_g. Let us define the gradient vectors of e_n and d_n with respect to p_g, which are shown in (13) and (14), respectively.

$$\nabla_p e_n = \left(\frac{\partial e_n}{\partial p_1}, \ldots, \frac{\partial e_n}{\partial p_G} \right) = (\alpha_{n,1}\gamma_1, \alpha_{n,2}\gamma_2, \ldots, \alpha_{n,G}\gamma_G) \tag{13}$$

$$\nabla_p d_n = \left(\frac{\partial d_n}{\partial p_1}, \ldots, \frac{\partial d_n}{\partial p_G} \right) = (\alpha_{n,1}, \alpha_{n,2}, \ldots, \alpha_{n,G}) \tag{14}$$

Now we can derive $\frac{\partial p_g}{\partial d_n}$ by using the gradient vectors as:

$$\frac{\partial e_n}{\partial d_n} = \frac{\nabla_p e_n \cdot \nabla_p d_n}{\|\nabla_p d_n\|^2}, \tag{15}$$

where $\nabla_p e_n \cdot \nabla_p d_n$ is the dot product of the two gradient vectors and $\|\nabla_p d_n\|^2$ is the squared magnitude (norm) of the gradient $\nabla_p d_n$.

The numerator and denominator of (15) are computed as:

$$\nabla_p e_n \cdot \nabla_p d_n = \sum_{g=1}^{G} (\alpha_{n,g}\gamma_g)(\alpha_{n,g}) = \sum_{g=1}^{G} \alpha_{n,g}^2 \gamma_g \tag{16a}$$

$$\|\nabla_p d_n\|^2 = \sum_{g=1}^{G} (\alpha_{n,g})^2 \tag{16b}$$

Substituting them back into (15), we can finally obtain the locational marginal carbon emission rate:

$$\frac{\partial e_n}{\partial d_n} = \frac{\sum_{g=1}^{G} \alpha_{n,g}^2 \gamma_g}{\sum_{g=1}^{G} \alpha_{n,g}^2} \tag{17}$$

B. Nomenclature

p_g	Power output of generator g.
γ_g	Carbon emission rate of generator g.
e_n	Carbon emission amount of node n.
e_n, t	Carbon emission amount of node n at time period t.
d_n	Power demand of node n.
$d_{n,g}$	Power demand of node n that is served by generator g.
δ_n	Average carbon emission rate of node n.
$\alpha_{n,g}$	Generator-to-load distribution factor for generator g to the load located on node n.
p_l	Power flow on transmission line l.

Acknowledgment

We gratefully acknowledge funding support from the California Energy Commission (Award EPC-20-025-FP12037) and the National Science Foundation (Award 2324940).

References

[1] U.S. Energy Information Administration. (2024, Apr.) U.S. energy-related carbon dioxide emissions, 2023. Release Date: April 25, 2024. Retrieved from https://www.eia.gov. [Online]. Available: https://www.eia.gov

[2] A. Hundiwale, "Greenhouse gas emission tracking methodology," *Technical Report, California ISO*, 2016.

[3] E. Lau, Q. Yang, A. Forbes, P. Wright, and V. Livina, "Modelling carbon emissions in electric systems," *Energy Conversion and Management*, vol. 80, pp. 573–581, 2014.

[4] K. Leerbeck, P. Bacher, R. G. Junker, G. Goranović, O. Corradi, R. Ebrahimy, A. Tveit, and H. Madsen, "Short-term forecasting of CO_2 emission intensity in power grids by machine learning," *Applied Energy*, vol. 277, p. 115527, 2020.

[5] W. Wang, Y. Li, and N. Yu, "Predict locational marginal greenhouse gas emission factors of electricity with spatial-temporal graph convolutional networks," in *2023 IEEE PES Innovative Smart Grid Technologies Europe (ISGT EUROPE)*, 2023, pp. 1–6.

[6] Y. Cheng, N. Zhang, B. Zhang, C. Kang, W. Xi, and M. Feng, "Low-carbon operation of multiple energy systems based on energy-carbon integrated prices," *IEEE Transactions on Smart Grid*, vol. 11, no. 2, pp. 1307–1318, 2019.

[7] B. Park, J. Dong, B. Liu, and T. Kuruganti, "Decarbonizing the grid: Utilizing demand-side flexibility for carbon emission reduction through locational marginal emissions in distribution networks," *Applied Energy*, vol. 330, p. 120303, 2023.

[8] K. E. Van Horn and D. Apostolopoulou, "Assessing demand response resource locational impacts on system-wide carbon emissions reductions," in *2012 North American Power Symposium (NAPS)*, pp. 1–6.

[9] Y. Wang, C. Wang, C. Miller, S. McElmurry, S. Miller, and M. Rogers, "Locational marginal emissions: Analysis of pollutant emission reduction through spatial management of load distribution," *Applied energy*, vol. 119, pp. 141–150, 2014.

[10] J. Lindberg, Y. Abdennadher, J. Chen, B. C. Lesieutre, and L. Roald, "A guide to reducing carbon emissions through data center geographical load shifting," in *Proceedings of the Twelfth ACM International Conference on Future Energy Systems*, 2021, pp. 430–436.

[11] C. Kang, T. Zhou, Q. Chen, J. Wang, Y. Sun, Q. Xia, and H. Yan, "Carbon emission flow from generation to demand: A network-based model," *IEEE transactions on smart grid*, vol. 6, no. 5, pp. 2386–2394, 2015.

[12] B. Li, Y. Song, and Z. Hu, "Carbon flow tracing method for assessment of demand side carbon emissions obligation," *IEEE Transactions on Sustainable Energy*, vol. 4, no. 4, pp. 1100–1107, 2013.
[13] Y. Chen, D. Deka, and Y. Shi, "Contributions of individual generators to nodal carbon emissions," in *Proceedings of the 15th ACM International Conference on Future and Sustainable Energy Systems*, 2024, pp. 415–421.
[14] X. Chen, A. Sun, W. Shi, and N. Li, "Carbon-aware optimal power flow," *arXiv preprint arXiv:2308.03240*, 2023.
[15] R. D. Zimmerman, C. E. Murillo-Sánchez, and R. J. Thomas, "MATPOWER: Steady-state operations, planning, and analysis tools for power systems research and education," *IEEE Transactions on power systems*, vol. 26, no. 1, pp. 12–19, 2010.
[16] Z. Shao, Q. Zhai, J. Wu, and X. Guan, "Data based linear power flow model: Investigation of a least-squares based approximation," *IEEE Transactions on Power Systems*, vol. 36, no. 5, pp. 4246–4258, 2021.